Journal of Medicinal Chemistry

Article

Design and Characterization of the First Selective and Potent Mechanism-Based Inhibitor of Cytochrome P450 4Z1

John P. Kowalski, Matthew G. McDonald, Robert D. Pelletier, Helmut Hanenberg, Constanze Wiek, and Allan E Rettie

J. Med. Chem., **Just Accepted Manuscript** • DOI: 10.1021/acs.jmedchem.0c00101 • Publication Date (Web): 17 Apr 2020

Design and Characterization of the First Selective and Potent Mechanism-Based Inhibitor of Cytochrome P450 4Z1

John P. Kowalski[†], Matthew G. McDonald[†], Robert D. Pelletier[†], Helmut Hanenberg[‡], Constanze Wiek[§], Allan E. Rettie[†,*]

[†]Department of Medicinal Chemistry, School of Pharmacy, University of Washington, Seattle, WA 98105, USA

[‡]Department of Pediatrics III, University Children's Hospital Essen, University of Duisburg-Essen, 45122 Essen, Germany

[§]Department of Otorhinolaryngology and Head/Neck Surgery, Heinrich-Heine University, 40225 Düsseldorf, Germany

*Corresponding author, email: rettie@uw.edu

Abstract

Mammary tissue-restricted cytochrome P450 4Z1 (CYP4Z1) has garnered interest for its potential role in breast cancer progression. CYP4Z1-dependent metabolism of arachidonic acid preferentially generates 14,15-epoxyeicosatrienoic acid (14,15-EET), a metabolite known to influence cellular proliferation, migration, and angiogenesis. In the present study, we developed time-dependent inhibitors of CYP4Z1 designed as fatty acid mimetics linked to the bioactivatable pharmacophore, 1-aminobenzotriazole (**ABT**). The most potent analog, 8-[(1H-benzotriazol-1-yl)amino]octanoic acid (**7**), showed a 60-fold lower shifted IC_{50} for CYP4Z1 compared to **ABT,** efficient mechanism-based inactivation of the enzyme evidenced by a K_I = 2.2 μM, k_{inact} = 0.15 min^{-1} and a partition ratio of 14. Furthermore, **7** exhibited low off-target inhibition of other CYP isozymes. Finally, low micromolar concentrations of **7** inhibited 14,15-EET production in T47D breast cancer cells transfected with CYP4Z1. This first-generation,

selective MBI will be a useful molecular tool to probe the biochemical role of CYP4Z1 and its association with breast cancer.

Introduction

Cytochrome P450 (CYP) enzymes are a critical family of hemoproteins that are involved in the metabolism of both xenobiotic and endogenous molecules.[1] In 2004, CYP4Z1 was cloned from a breast carcinoma line and subsequently shown by several groups to be up-regulated in breast carcinoma.[2,58,59] Other expression profiling studies also demonstrate consistently that CYP4Z1 transcript level is associated with an elevated tumor grade and increased tumor aggressiveness.[56,57,60] Some mechanistic insight has been provided by the finding that overexpression of CYP4Z1 promotes angiogenesis and tumor growth both *in vitro* and *in vivo*[3].

Many CYP4 enzymes are capable of metabolizing polyunsaturated fatty acids (PUFAs) to biological compounds that participate in a complex web of signaling.[4] Key metabolites of arachidonic acid (AA, **Fig. 1**), namely 20-hydroxyeicosatetraenoic acid (20-HETE) and 14,15-epoxyeicosatrienoic acid (14,15-EET), are thought to play roles in human cancer progression, by influencing angiogenesis, tumor growth and metastasis.[5-7] We recently established that 14,15-EET is a dominant metabolite of CYP4Z1-dependent AA metabolism and have speculated that a role for CYP4Z1 in breast cancer may involve this signaling ligand.[8]

Breast cancer is one of the leading causes of death in women, with more than 2 million new cases diagnosed worldwide in 2018.[9] Novel therapeutic modalities are needed urgently, especially for recurrent and metastatic tumors.[10] Endogenous mammary-specific expression of CYP4Z1 offers a new avenue to explore for breast cancer treatment, and there has already

been success with CYP inhibitors developed for anti-cancer therapy. For example, aromatase (CYP19) inhibitors, such as exemestane, letrozole and anastrozole, are useful in breast cancer treatment because they effectively limit estrogen production.[11]

Therefore, the goal of this study was to develop a potent and selective mechanism-based inhibitor (MBI) of CYP4Z1 to enable biochemical characterization of this enzyme and help unravel the role that bioactive lipid metabolites play in breast cancer progression. Herein, we show that analogs of 1-aminobenzotriazole (**ABT**) are potent time-dependent inhibitors of CYP4Z1. Two analogs (**6, 7**) showed pronounced selectivity as reversible inhibitors of CYP4Z1, compared to other CYP enzymes, and even higher selectivity when they were evaluated for their time-dependent effects on off-target CYPs. Further, we confirmed mechanism-based inhibition for our most potent and selective analog, 8-[(1H-benzotriazol-1-yl)amino]octanoic acid (**7**), determined the kinetics of inactivation, and assessed the potency of **7** towards inhibition of CYP4Z1-mediated 14,15-EET production in a breast cancer cell line.

Results and Discussion

CYP4Z1 Assay for Rapid Inhibitor Screening. A mammalian enzyme source was preferred and, historically, HepG2 cells have been suitable for heterologous expression of CYPs due to their very low basal CYP levels and catalytically sufficient amounts of the co-enzymes cytochrome P450 reductase and cytochrome b5.[12,13] Therefore, a CYP4Z1-expressing HepG2 cell line was generated via lentiviral transduction (**Figure S1A**) and membranes prepared from these cells to use as the primary enzyme source for screening. This expression system provided an adequate amount of CYP4Z1, with no detectable enzyme in a control vector cell line, as analyzed by western blot (**Figure S1B**). Quantification *via* carbon monoxide-binding

spectra[14] showed that HepG2 membrane preparations contained 1 μM of active CYP4Z1 enzyme (**Figure S1D**). To test for CYP4Z1 inhibition, we established a simple, sensitive functional assay using the recently identified CYP4Z1 substrate luciferin-benzyl ether[15] (Luc-BE, **Figure 1**). Utilization of this probe substrate enabled higher throughput evaluation of inhibitor potency versus the use of more technically cumbersome fatty acid(s) such as laurate and arachidonate.[8] Luc-BE turnover to its luminescent metabolite, luciferin, is easily analyzed with Promega's P450 Glo kit.[16] The reaction is NADPH-dependent, turnover is >500-fold higher than background (**Figure 2A)** and displays apparent Michaelis-Menten kinetics (**Figure 2B**). For determination of half maximal inhibitory concentration (IC_{50}) values for CYP4Z1 inhibition, the probe substrate Luc-BE was used at a concentration equal to the determined K_m (29 μM). To evaluate both the reversible, and time-dependent nature of potential inhibitors, we used a non-dilution (also termed addition) method IC_{50} shift assay.[17 – 19] Typically, if a compound elicits an IC_{50} shift of ≥1.5 it is considered to be a time-dependent inhibitor of the enzyme being evaluated.[20]

Design and Synthesis of ABT-analogs for CYP4Z1 Inhibition. We undertook a targeted design strategy for a CYP4Z1 mechanism-based inhibitor in order to capitalize on potential selectivity benefits. The rationale for increased specificity is based on the following features: i) reversible binding of the inhibitor to the enzyme must be of appropriate affinity, ii) the inhibitor must also serve as a substrate for bioactivation by the target, and iii) the reactive metabolite that is generated requires an active site target to inactivate the enzyme.[1,21]

The known inhibitors of CYP4Z1 are promiscuous towards the CYP4 family and other hepatic CYP enzymes.[8,15] Our preliminary work demonstrated that **ABT**, a mechanism-based pan-CYP inhibitor,[21,22] displayed significant time-dependent inhibition of CYP4Z1. Thus, **ABT**

appeared to offer a promising bioactivatable pharmacophore, and our data agreed with prior research, which indicated that **ABT** effectively inactivates AA-oxidizing CYPs.[23] Additionally, there was already considerable precedent for exploration of ABT-analogs, as prior studies have characterized *N*-benzyl-aminobenzotriazole, *N*-α-methylbenzyl-aminobenzotriazole, and *N*-α-ethylbenzyl-aminobenzotriazole as isozyme-selective MBIs of rabbit, guinea pig, and rat CYPs.[24 – 26,53]

CYP4B1 is the only CYP4 member that has been crystallized,[27] therefore, structural inferences that can be made about CYP4Z1 are limited. However, catalytic work with CYP4Z1 provided a useful basis for simple inhibitor design. Unlike most other CYP4 enzymes, CYP4Z1 catalyzes oxidations internally rather than at the ω-terminus.[8,15,54] In addition to AA metabolism, the internal preference for oxidation is evident for the substrates lauric acid (LA) and Luc-BE (**Figure 1**). Therefore, we made simple chemical modifications to the **ABT** scaffold to generate CYP4Z1 inhibitors by adding carbon tails to **ABT** to incorporate structural elements of the known CYP4Z1 substrate, LA. Ideally, we wanted to take advantage of the relatively high mid-chain oxidation rate of LA to 8-hydroxy-LA (V_{max} = ~40 min^{-1}) in the hope that this would translate to CYP4Z1-mediated bioactivation of ABT-analogs. The position of the exocyclic nitrogen that was expected to undergo P450-mediated activation in these new *N*-alkylated **ABT** congeners approximates the internal site of CYP4Z1-dependent metabolism of LA. Moreover, as illustrated by the docking of LA to the recently published CYP4Z1 homology model,[8] hydrophilic residues Asn381 and Ser383 are positioned to potentially engage with the free acid moiety of fatty acid substrates. This hypothesis was tested by evaluating ABT-analog inhibitors which contained a terminal carboxylic acid group alongside inhibitors where that moiety had been removed.

Neutral chain analogs were prepared from readily available aliphatic aldehyde building blocks using methodology based on that previously used in the synthesis of *N*-benzyl-aminobenzotriazole.[24] Acid-containing analogs were synthesized using terminal acid, primary alcohol starting materials and employing PCC-mediated oxidation to generate the aldehyde moiety. Condensation of the aldehyde with **ABT** formed an imine which was then reduced to the target compounds (**Scheme 1**).

Evaluation of Time-Dependent Inhibition (TDI) of CYP4Z1 by ABT-analogs. Representative dose-response curves are provided in **Figure 3**, which shows the potency comparison between **ABT** and inhibitor **7** (all dose-response curves have been provided in the Supporting Information, **Figure S2**). IC_{50} values for all ABT-analogs are shown in **Table 1**. **ABT** itself only weakly inhibited CYP4Z1 without a prior pre-incubation with NADPH. However, the addition of aliphatic tails (compounds **1** – **5**) dramatically increased affinity for CYP4Z1 over that of **ABT**, exemplified by a 50-fold decrease in the reversible IC_{50} value from 154 to 2.9 μM for inhibitor **2**. While **ABT** itself showed a potent time-dependent effect for inhibition of CYP4Z1 (i.e. a 30-minute pre-incubation of NADPH with CYP4Z1 produced a shifted-IC_{50} of 12 μM), inhibitors **2-9** exhibited much lower shifted-IC_{50} values that indicated up to 120-fold higher potency compared to **ABT**.

Analysis of the terminal acid-containing analogs showed similar gains in affinity over **ABT** itself for CYP4Z1 inhibition. The most potent congeners, **7** and **8 (**with eight and ten carbon tails respectively), exhibited shifted-IC_{50} values of 200 nM, *i.e.* a 60-fold increase in potency over **ABT**. Interestingly, the addition of the acid moiety did not have a dramatic effect on CYP4Z1 inhibition potency (neither affinity nor inactivation) compared to the neutral-chain aliphatic variants. However, the benefits of adding a terminal acid group became apparent as

counter-screening proceeded as described below. Finally, despite changes in apparent potencies for reversible and time-dependent inhibition across the entire analog series, the shift ratios (IC_{50} / Shifted-IC_{50}) varied only from 13 – 30 (omission of **3** narrowed this range to 23 – 30), which seems consistent with all inhibitors inactivating CYP4Z1 via a common mechanism.

Counter-Screening Against CYP4 Family Enzymes. Due to the complex nature of the role that fatty acid metabolites play in signaling in both healthy and disease states,[4,5] non-specific CYP4Z1 inhibitors such as **ABT**[15,23] and HET0016[3,8,28,29] do not provide adequately discriminatory molecular tools with which to assess the physiological role of CYP4Z1. Consequently, we next evaluated the selectivity of the new ABT-analogs against recombinantly-expressed, and commercially available, CYP4 enzymes; CYP4A11, -4F2, -4F3a, -4F3b, and -4F12. As it is not commercially available, but was still of interest to us, CYP4F8 was expressed in HepG2 cells and membranes were prepared identically to that for CYP4Z1. Pro-luciferin probe substrates at concentrations $\leq K_m$ (see Experimental Section) were used for all CYP4 isozymes to determine inhibition, including CYP4F8 (as elucidated from in-house testing, **Figure S8**), an isozyme in which limited substrate information has been published. A TDI assay at a single, moderate, concentration of 30 μM was utilized in order to assess whether any analogs significantly inhibited the off-target enzymes. A 30-minute enzyme/NADPH pre-incubation step was used to assess time-dependent effects (akin to a full IC_{50}-shift assay), which were modest for all enzymes and analogs tested (**Figure 4**). Initial screening against off-target CYP4 isozymes was performed with inhibitors **2 – 9** (inhibitor **1** was excluded due to its low potency). The alkyl-modified analogs **2** – **5** inhibited CYP4F2, CYP4F3a and b and CYP4F12 substantially, whereas the acid modified analogs containing 10 and 12 carbon tails, **8** and **9**, respectively, substantially inhibited CYP4A11, CYP4F8 and 4F12. Importantly, however, two acid analogs **6** and **7** exhibited negligible or very low activity towards the CYP4 enzymes tested and were therefore selected for further study.

Evaluation of TDI for Inhibitors 6 and 7 Against Off-target CYP isozymes. Full IC_{50}-shift assays (**Figures S3, S4**) were performed with **6** and **7** to thoroughly assess off-target inhibition towards the other recombinantly-expressed CYP4 enzymes (**Table 2**). As determined from the specificity ratios (off-target CYP IC_{50} / CYP4Z1 IC_{50}), both **6** and **7** were comparatively poor reversible inhibitors of these isozymes compared to CYP4Z1. Relatively small shift ratios (~1-3) were obtained for both inhibitors against the six CYP4 isozymes tested, indicating low propensity of **6** and **7** for enzyme-mediated bioactivation. Of note, any shift values <1 (indicative of inhibitors with lowered potency after a plus NADPH pre-incubation) likely result from significant metabolism of the inhibitor by the CYP to non-bioreactive species. The contrasting reactivity of **6** and **7** between these off-target isozymes and CYP4Z1 is readily apparent from the resultant TDI specificity ratios (off-target CYP shifted-IC_{50} / CYP4Z1 shifted-IC_{50}) that ranged from 137 to 2235. Therefore, CYP4Z1 selectivity becomes greatly enhanced as the result of TDI for these two inhibitors.

Overall, inhibitor **7** possessed a higher degree of selectivity for CYP4Z1 than **6.** Additionally, although **7** showed relatively similar affinity across the off-target CYP4 isozymes, only CYP4F8 and CYP4F12 were well above the significance threshold for TDI (i.e. shift ratio $\geq$ 1.5). This indicates that these two enzymes are more likely to bind **7** in a position which leads directly to bioactivation. We suggest that this is the result of structural similarities with CYP4Z1 that are not present in the other CYP4 enzymes tested, namely, a lack of the active site glutamate residue necessary to form a covalent attachment with the heme.[8] The recent publication on the crystal structure of octane-bound CYP4B1, an ω-hydroxylase with a covalently attached heme, showed that this structural element is an important determinant of the enzyme's (and most likely other similar CYP4 isozymes) regio-specificity for oxidation at the

terminal position of alkyl-chain containing substrates.[27] Indeed, both CYP4F8 and CYP4F12 enzymes, neither of which possess a covalently attached heme, primarily produce an internal ω-3-hydroxylated AA metabolite, 18-HETE,[30,31] and thus seem to more closely mimic CYP4Z1 than the 20-HETE producing CYP4 family members. However, although the shift ratios pass the threshold of significance for these two isozymes, they are ~10-fold lower than the shift ratio observed for **7** and CYP4Z1. This results in CYP4F8 and CYP4F12 being inhibited 285-fold and 230-fold less, respectively, than CYP4Z1 after a pre-incubation with cofactor. We speculate that this observation reflects the fact that 18-HETE is still three to four C-C bond lengths away from the major site of CYP4Z1-mediated AA metabolism, and thus bioactivation of **7** is limited for CYP4F8 and CYP4F12 because the exocyclic nitrogen for this analog is not positioned optimally for these two isozymes.

Full IC_{50}-shift assays were also performed with **6** and **7** to evaluate off-target inhibition towards hepatic CYP isozymes (**Figures S5, S6**), chosen based on the seven FDA recommended CYPs for drug-drug interaction (DDI) testing.[32] Human liver microsomes (HLM) served as the enzyme source and a cocktail method was employed to evaluate inhibition of CYP1A2, -2B6, -2C8, -2C9, -2C19, -2D6, and -3A4/5 concurrently (**Table 3**). Of note, in-house testing for inhibition, using isozyme-specific inhibitor probes, of metabolism by the seven hepatic CYPs in the cocktail assays yielded data in agreement with that reported in the literature[33] (**Figure S9**). Similar to the results obtained with the CYP4 isozymes, inhibitors **6** and **7** did not potently inhibit off-target hepatic CYPs, either reversibly or irreversibly, with specificity and TDI specificity ratios spanning 23 – 140 and 134 – 1650, respectively. For both inhibitors, the largest shift ratios were observed for CYP1A2, at 12.2 and 11.2 for **6** and **7**, respectively. The large degree of bioactivation observed may be explained by CYP1A2, like CYP4Z1, having a propensity itself for internal oxidation of PUFAs. The 14,15-EET synthase activity for CYP1A2 has been reported to be ~0.54 pmol/pmol/min (at 50 μM AA),[34,35] and is in a similar range to that

observed for CYP4Z1 of 1.9 pmol/pmol/min (at 75 μM AA).[8] Furthermore, all seven of the hepatic CYP isozymes that we analyzed have been shown previously to metabolize AA to 14,15-EET, albeit with a large range of efficiencies and regio-specificities.[35] Although for most AA-metabolizing CYPs their role in breast cancer progression is largely unknown, CYP3A4 expression has been specifically linked to decreased survival and is required for growth in several breast cancer cell lines.[36] Therefore, the low off-target inhibition of the generally liver-localized CYPs studied herein was a desired trait for both broad selectivity purposes and will also allow for discriminatory probing of the role of CYP4Z1-dependent epoxygenase activity in a breast cancer setting. Overall, both inhibitors **6** and **7** demonstrated their lack of activity towards off-target enzymes primarily through low rates of bioactivation that resulted in modest time-dependent inhibition and high TDI specificity ratios. Due to its combined properties of high potency and excellent selectivity for CYP4Z1, inhibitor **7** was chosen for in-depth characterization as an MBI.

Characterization of Mechanism-based Inactivation of CYP4Z1 by 7. Mechanism-based inactivation is typically viewed as a characteristic to be designed away from in drug development, as the enzymes affected by this process are frequently off-target CYPs. When this occurs, DDIs are common liabilities as these off-target enzymes are rendered catalytically incompetent and must then be newly biosynthesized. However, numerous irreversible inhibitors (including MBIs) have emerged recently as therapeutics and have the benefits of increased biochemical efficiency, a longer duration of action, efficient inactivation of the target, and the potential to avoid some resistance mechanisms.[37] Examples of CYP MBI drugs include some aromatase (CYP19A) inhibitors that have shown efficacy in the clinic and are currently used for breast cancer treatment; an example being the steroidal mimetic exemestane.[38] Evaluating the

characteristics of an MBI (not simply establishing TDI) enables insight into inhibitor structure-activity relationships, mechanisms of action, guides future analog work, and provides a better understanding of the biochemistry of the target CYP. Therefore, the action of inhibitor **7** towards CYP4Z1 was considered in light of the Silverman criteria for an MBI.[39]

As seen in **Figure 5A**, **7** displayed concentration- and time-dependent loss of enzyme activity, as first indicated by the single time point assays described above. When the values for k_{obs} were plotted against concentrations of **7**, a K_I = 2.2 μM and a k_{inact} = 0.15 min^{-1} (**Figure 5B**) were determined; the observed maximal rate of inactivation indicating saturation kinetics. Comparison with exemestane, where a k_{inact} for aromatase inhibition of 0.05 min^{-1} has been determined, emphasizes how rapidly **7** inactivates CYP4Z1, although it must be noted that exemestane inactivation of aromatase is highly efficient due to its tight-binding affinity (K_I = 26 nM) for the enzyme.[40] In order to show irreversibility of mechanism-based inactivation, we assessed the fraction of activity remaining, from CYP4Z1 treated with **7**, before and after overnight dialysis to remove excess inhibitor (**Figure 5C**). No increased activity was observed after dialysis, indicating irreversible enzyme destruction. Multiple experiments confirmed the necessity of a catalytic step for the time-dependent inhibition of CYP4Z1 by **7**. This is directly shown in the dialysis experiment where lack of a pre-incubation step with the NADPH cofactor prior to the substrate turnover reaction resulted in no inactivation of the enzyme. The addition of hard or soft nucleophiles, at commonly used concentrations for reactive intermediate trapping experiments[41] – glutathione (GSH), *N*-acetyl lysine (NAL), methoxyamine ($MeONH_2$), *N*-acetyl cysteine (NAC), semicarbazide (Semicarb.), potassium cyanide (KCN) – did not abrogate inactivation of CYP4Z1 by **7** (**Figure 5D**). Additionally, the presence of the reactive oxygen species scavenging enzymes, catalase (CAT) and superoxide dismutase (SOD), did not rescue CYP4Z1 activity, eliminating the possibility of non-specific, and non-enzymatic, oxidation

reactions causing inactivation of CYP4Z1. These data indicate that inactivation of CYP4Z1 occurs prior to release of bioactivated **7** from the active site.

Next, the partition ratio for inactivation of CYP4Z1 by **7** was determined (**Figure 5E**). As a measure of efficiency, the partition ratio is the number of latent inactivator molecules converted and released as a product relative to each catalytic cycle resulting in enzyme inactivation.[39,42] Partition ratios for MBIs of CYPs can span a large range, with values reported from 1 to >5000.[43] Therefore, the partition ratio of 14 for **7** lies towards the efficient end of this spectrum.

Inhibition of CYP4Z1 AA metabolism in T47D Cells by 7. We next evaluated the inhibition of CYP4Z1-dependent metabolism of AA in breast cancer derived T47D cells.[44] Although a low level of CYP4Z1 mRNA is detectable in breast cancer cell lines, which may be induced ~15-fold from dexamethasone treatment,[55] immortalization appears to eliminate expression of endogenous CYP4Z1.[3] Therefore, T47D cells were modified to constitutively express CYP4Z1 (T47D-CYP4Z1) using a recombinant lentivirus. Western blot analysis showed ample CYP4Z1 expression in the CYP4Z1-T47D cells and no observable endogenous CYP4Z1 expression in the Vector-T47D cells (**Figure S1C**). Concentrations of free AA in human plasma span a wide range, from 2.7 to 50 μM.[45,46] Therefore, a 50 μM dose of AA was used to reflect this upper boundary. The previously characterized CYP4Z1 metabolites of AA, 19-HETE and 14,15-EET, along with the metabolite commonly generated by other CYP4 isozymes, 20-HETE, were monitored.[8] Also included in the AA metabolite profile was the degradation product 14,15-dihydroxy eicosatrienoic acid (14,15-DiHET), as this could be generated by 14,15-EET hydrolysis both non-enzymatically, in the tissue culture environment, and enzymatically through the action of epoxide hydrolases potentially present in T47D cells.[35,47]

The T47D-CYP4Z1 cells were exposed to **7**, incorporating a 24-hour inhibitor pre-incubation step prior to introduction of substrate, to assess TDI. At 3 μM, potent inhibition of AA metabolism was observed (**Figure 6**). Comparing peak area ratios (PAR), of metabolites divided by their respective deuterated internal standards, showed that production of 14,15-EET, 19-HETE, and 14,15-DiHET was inhibited 83, 86, and 80%, respectively. When inhibitor and substrate were administered together to T47D-CYP4Z1 cells, without a pre-incubation step, 3 μM of **7** produced lower levels of inhibition against production of 14,15-EET, 19-HETE, and 14,15-DiHET, (**Table 6**), as expected. When dosed at 1 μM, a comparable time-dependent effect was observed with a ~2-fold decrease in potency. Similar results were also attained when investigating AA metabolism in CYP4Z1-HepG2 membranes, where a time-dependent, ~90% loss in CYP4Z1 activity (**Figure S10)** was observed with inhibitor **7** utilized at 3 μM**.**

Finally, we confirmed the preference for CYP4Z1-mediated 14,15-EET production over that of 20-HETE (only a trace amount was detected, slightly above lower limit of detection) in a mammalian whole cell setting. Although other internal oxidation products from CYP4Z1 AA metabolism were observed in both the HepG2 membranes and T47D cells (decreasing proportionally with inhibitor and tentatively identified as 15-, 16-, 17-, and 18-HETE), these apparently minor metabolites were not characterized further here.

These data demonstrate the efficacy of inhibitor **7** in a whole cell environment, and are comparable to results we obtained for the inhibition of CYP4Z1-mediated Luc-BE *O*-debenzylation in HepG2 cells (**Figure S11A**). Therefore, although not tested directly, potentially lower inhibitor permeability and stability in whole cells appear not to be major issues. Additionally, these results are not confounded by possible cytotoxicity of inhibitor **7**, as a 3 μM treatment did not cause noticeable changes in viability 24 hours later for any of the cell lines assayed (**Figure S11B**). Although we hypothesize **7** to have anti-proliferative effects against

breast cancer cells expressing CYP4Z1, the specific conditions required to capture this effect (e.g. temporal, growth factor, and PUFA substrate variables) were not assessed here as it was beyond the scope of this study. To our knowledge, no studies utilizing primary cells have been performed to interrogate CYP4Z1. However, due to its effectiveness in a breast-cancer derived cell line for inhibiting the generation of the pro-angiogenic and pro-proliferative metabolite 14,15-EET, we posit that inhibitor **7** will be an effective molecular tool to probe the druggability of CYP4Z1 as a target for breast cancer therapy in varied *in vitro* settings.

Conclusion

In summary, we leveraged our knowledge of the product selectivity of CYP4Z1 to generate ABT-analogs that are efficient time-dependent inhibitors of the enzyme with substantially increased potency over **ABT**. The design strategy of incorporating a terminal acid to produce fatty acid mimetics resulted in high selectivity for CYP4Z1 for two analogs, **6** and **7**. Further characterization, monitoring isozyme-specific inhibition in a large panel of off-target CYPs, identified **7** as the inhibitor with the best combination of isozyme selectivity and potency. **7** was further characterized as a relatively efficient mechanism-based inhibitor (k_{inact}/K_i = 0.07 $min^{-1}\mu M^{-1}$), with demonstrated time-dependent inhibition of CYP4Z1 in transfected breast cancer-derived whole cells.

Future studies will investigate the mechanism of CYP4Z1 inactivation by **7** through trapping of reactive metabolite(s) and analysis of heme and apoprotein adducts. These first-generation inhibitors are potentially useful lead compounds for the development of more potent CYP4Z1 inhibitors with appropriate pharmacokinetic features to support *in vivo* studies and potential clinical applicability.

Experimental Section

General Information for Synthesis. All solvents and reagents were purchased from commercial sources (Alfa Aesar, Acros Organics, AstaTech, Fisher, Oakwood Chemical, Sigma-Aldrich, and TCI) and used as received. All reactions were monitored by thin-layer chromatography, visualized by either UV (254 nm) or potassium permanganate stain. For isolation of purified compounds, normal phase chromatography was carried out on a Teledyne Isco Combiflash system (Lincoln, NE). ^{1}H and ^{13}C NMR spectra were recorded at 25 °C in deuterated chloroform ($CDCl_3$) on either a 499.73 MHz Agilent DD2 (Santa Clara, CA) or 499.96 MHz Bruker Avance series (Billerica, MA) spectrometer, respectively. Chemical shifts are reported below relative to the solvent peak in $CDCl_3$ at 7.26 ppm (^{1}H NMR), or tetramethylsilane at 0.00 ppm (^{13}C NMR). Coupling constants (*J*) are noted in hertz (Hz), and peak multiplicities as either a singlet (s), doublet (d), triplet (t), pentet (p), or multiplet (m). All ^{1}H and ^{13}C NMR spectra have been provided in the Supporting Information. Accurate mass and purity analyses of the synthesized compounds were determined via UPLC−MS on a Waters Acquity UPLC (Milford, MA) coupled in tandem with a Waters Acquity tunable UV detector and a Thermo LTQ-Orbitrap mass spectrometer (San Jose, CA). Purity as assessed by UPLC−UV (254 and 280 nm) and ^{1}H NMR spectroscopy were ≥ 95% for all compounds.

Alcohol Oxidation (General Procedure I). A modified version of an existing method that has been published was utilized[48] and was as follows: A dried and N_2-purged round-bottom flask containing 1-2 g celite was charged with pyridinium chlorochromate (PCC, 3-5 mmol, 1.5 eq), solvated in ~50 mL anhydrous dichloromethane. The appropriate primary alcohol (2-3 mmol), solvated in a minimal amount of anhydrous dichloromethane, was subsequently added to the reaction flask, and the mixture was stirred at room temperature under N_2 for 90 minutes. Next, anhydrous diethyl ether was added to the slurry and the mixture was filtered through a pad of celite, rinsed with several portions of diethyl ether, and solvent was removed from the combined organic fractions under vacuum. The residue was then washed thrice with portions of

diethyl ether to harvest the soluble oxo-product and the combined diethyl ether fractions were once again filtered through celite and solvent was removed under vacuum to afford the corresponding aldehyde.

Imine Formation (General Procedure II). Modified versions of existing methods that have been published were utilized for both general procedures II and III[24] and were as follows: A dried and N_2-purged round-bottom flask was charged with **ABT** (0.75 mmol), the appropriate aldehyde (4.5 mmol, 6.0 eq), and ~20 mL glacial acetic acid. For inhibitors **6** – **9**, the oxo-product derived from general procedure I (0.5-0.8 mmol) was reacted with 1.5 eq of **ABT**. The reaction mixture was stirred at room temperature overnight and the acetic acid was subsequently removed under vacuum. The crude product was purified via flash chromatography using a dichloromethane/ethyl acetate gradient to afford the corresponding imine intermediate (for analogs containing terminal carboxylic acid groups, 2% acetic acid was added to the mobile phase for improved chromatographic separation).

Imine Reduction (General Procedure III). A dried round-bottom flask was charged with the appropriate imine intermediate (0.3-0.7 mmol), $NaBH_4$ (~20 eq), and ~40 mL of a 2:1 solution of methanol/dichloromethane. The reaction mixture was stirred at room temperature for 1 hour and then the solvents were removed under vacuum. The remaining mixture was solvated in a 20:1 solution of dichloromethane/methanol and then washed thrice with H_2O; for the carboxylic acid-containing analogs, the H_2O was adjusted with 1N HCl to a pH of ~2 prior to washing. The organic fraction was dried over Na_2SO_4, filtered, and the crude product was purified via flash chromatography using a hexane/ethyl acetate gradient to afford the corresponding inhibitors **1 – 9.**

*N-butyl-1H-1,2,3-benzotriazol-1-amine (**1**).* Synthesized from butanal and **ABT** according to general procedures II and III, with respective yields of 89 and 80%. ^{1}H NMR (500 MHz, $CDCl_3$) δ 8.02 (d, J = 8.4 Hz, 1H), 7.61 (d, J = 8.3, 1H), 7.50 (t, J = 7.9 1H), 7.37 (t, J = 7.4, 1H),

3.42 (t, *J* = 7.1, 2H), 1.52 (p, *J* = 7.0, 2H), 1.46 (sx, *J* = 7.5, 2H), 0.93 (t, *J* = 7.2, 3H); ^{13}C NMR (125 MHz, $CDCl_3$) δ 144.4, 132.3, 127.7, 124.1, 119.9, 109.8, 52.91, 29.91, 19.96, 13.80; HRMS (ESI+) *m/z* [M+H] calculated ($C_{10}H_{15}N_4$) 191.1291, observed 191.1292, δ ppm 0.5.

*N-hexyl-1H-1,2,3-benzotriazol-1-amine (**2**).* Synthesized from hexanal and **ABT** according to general procedures II and III, with respective yields of 80 and 84%. ^{1}H NMR (500 MHz, $CDCl_3$) δ 8.02 (d, *J* = 8.4 Hz, 1H), 7.61 (d, *J* = 8.3, 1H), 7.50 (t, *J* = 7.5 1H), 7.37 (t, *J* = 7.2, 1H), 3.41 (t, *J* = 7.2, 2H), 1.53 (p, *J* = 7.3, 2H), 1.42 (p, *J* = 8.2, 2H), 1.29 (m, 4H), 0.88 (t, *J* = 6.9, 3H); ^{13}C NMR (125 MHz, $CDCl_3$) δ 144.4, 132.3, 127.6, 124.1, 119.9, 109.8, 53.22, 31.53, 27.84, 26.45, 22.52, 13.97; HRMS (ESI+) *m/z* [M+H] calculated ($C_{12}H_{19}N_4$) 219.1604, observed 219.1606, δ ppm 0.9.

*N-octyl-1H-1,2,3-benzotriazol-1-amine (**3**).* Synthesized from octanal and **ABT** according to general procedures II and III, with respective yields of 77 and 70%. ^{1}H NMR (500 MHz, $CDCl_3$) δ 8.00 (d, *J* = 8.4 Hz, 1H), 7.60 (d, *J* = 8.3, 1H), 7.48 (t, *J* = 7.3 1H), 7.35 (t, *J* = 7.2, 1H), 3.40 (t, *J* = 7.2, 2H), 1.52 (p, *J* = 7.3, 2H), 1.40 (p, *J* = 7.6, 2H), 1.26 (m, 8H), 0.87 (t, *J* = 7.1, 3H); ^{13}C NMR (125 MHz, $CDCl_3$) δ 144.4, 132.3, 127.7, 124.1, 119.9, 109.8, 53.27, 31.77, 29.31, 29.17, 27.88, 26.79, 22.62, 14.06; HRMS (ESI+) *m/z* [M+H] calculated ($C_{14}H_{23}N_4$) 247.1917, observed 247.1922, δ ppm 2.0.

*N-decyl-1H-1,2,3-benzotriazol-1-amine (**4**)*. Synthesized from decanal and **ABT** according to general procedures II and III, with respective yields of 67 and 70%. ^{1}H NMR (500 MHz, $CDCl_3$) δ 8.01 (d, *J* = 8.0 Hz, 1H), 7.60 (d, *J* = 8.3, 1H), 7.49 (t, *J* = 7.2 1H), 7.36 (t, *J* = 8.1, 1H), 3.40 (t, *J* = 6.8, 2H), 1.52 (p, *J* = 7.1, 2H), 1.41 (p, *J* = 6.9, 2H), 1.25 (m, 12H), 0.87 (t, *J* = 7.2, 3H); ^{13}C NMR (125 MHz, $CDCl_3$) δ 144.4, 132.3, 127.6, 124.1, 119.9, 109.8, 53.24, 31.88, 29.52, 29.35, 29.28, 27.89, 26.79, 22.67, 14.10; HRMS (ESI+) *m/z* [M+H] calculated ($C_{16}H_{27}N_4$) 275.2230, observed 275.2234, δ ppm 1.5.

*N-dodecyl-1H-1,2,3-benzotriazol-1-amine (**5**).* Synthesized from dodecanal and **ABT** according to general procedures II and III, with respective yields of 65 and 74%. ^{1}H NMR (500 MHz, $CDCl_3$) δ 8.02 (d, *J* = 8.4 Hz, 1H), 7.61 (d, *J* = 8.3, 1H), 7.50 (t, *J* = 7.7 1H), 7.37 (t, *J* = 7.3, 1H), 3.41 (t, *J* = 7.2, 2H), 1.53 (p, *J* = 7.4, 2H), 1.41 (p, *J* = 7.6, 2H), 1.25 (m, 16H), 0.88 (t, *J* = 6.9, 3H); ^{13}C NMR (125 MHz, $CDCl_3$) δ 144.4, 132.3, 127.7, 124.1, 119.9, 109.8, 53.28, 31.92, 29.63, 29.56, 29.52, 29.35, 27.89, 26.79, 22.69, 14.11; HRMS (ESI+) *m/z* [M+H] calculated ($C_{18}H_{31}N_4$) 303.2543, observed 303.2546, δ ppm 1.0.

*6-[(1H-1,2,3-benzotriazol-1-yl)amino]hexanoic acid (**6**).* Synthesized from 6-hydroxyhexanoic acid and **ABT** according to general procedures I, II and III, with respective yields of 23, 50 and 76%. ^{1}H NMR (500 MHz, $CDCl_3$) δ 8.01 (d, *J* = 8.4 Hz, 1H), 7.60 (d, *J* = 8.3, 1H), 7.49 (t, *J* = 7.8 1H), 7.36 (t, *J* = 7.9, 1H), 3.42 (t, *J* = 6.8, 2H), 2.36 (t, *J* = 7.3, 2H), 1.66 (p, *J* = 7.4, 2H), 1.52 (m, 4H); ^{13}C NMR (125 MHz, $CDCl_3$) δ 178.7, 144.3, 132.3, 127.9, 124.3, 119.9, 109.8, 52.87, 33.74, 27.56, 26.19, 24.34; HRMS (ESI+) *m/z* [M+H] calculated ($C_{12}H_{17}N_4O_2$) 249.1346, observed 249.1357, δ ppm 4.4.

*8-[(1H-1,2,3-benzotriazol-1-yl)amino]octanoic acid (**7**).* Synthesized from 8-hydroxyoctanoic acid and **ABT** according to general procedures I, II and III, with respective yields of 25, 60 and 80%. ^{1}H NMR (500 MHz, $CDCl_3$) δ 8.02 (d, *J* = 8.4 Hz, 1H), 7.60 (d, *J* = 8.3, 1H), 7.49 (t, *J* = 7.8 1H), 7.36 (t, *J* = 7.5, 1H), 3.40 (t, *J* = 7.1, 2H), 2.34 (t, *J* = 7.5, 2H), 1.63 (p, *J* = 7.3, 2H), 1.53 (p, *J* = 7.4, 2H), 1.43 (p, *J* = 6.7, 2H), 1.33 (m, 4H); ^{13}C NMR (125 MHz, $CDCl_3$) δ 179.3, 144.3, 132.3, 127.8, 124.3, 119.8, 109.8, 53.13, 33.99, 28.91, 28.88, 27.75, 26.53, 24.56; HRMS (ESI+) *m/z* [M+H] calculated ($C_{14}H_{21}N_4O_2$) 277.1659, observed 277.1670, δ ppm 4.0.

*10-[(1H-1,2,3-benzotriazol-1-yl)amino]decanoic acid (**8**).* Synthesized from 10-hydroxydecanoic acid and **ABT** according to general procedures I, II and III, with respective

yields of 21, 43 and 56%. ^{1}H NMR (500 MHz, $CDCl_3$) δ 8.01 (d, *J* = 8.4 Hz, 1H), 7.60 (d, *J* = 8.3, 1H), 7.49 (t, *J* = 7.8 1H), 7.36 (t, *J* = 7.5, 1H), 3.40 (t, *J* = 7.1, 2H), 2.34 (t, *J* = 7.5, 2H), 1.62 (p, *J* = 7.4, 2H), 1.52 (p, *J* = 7.5, 2H), 1.40 (p, *J* = 6.7, 2H), 1.28 (m, 8H); ^{13}C NMR (125 MHz, $CDCl_3$) δ 179.2, 144.3, 132.2, 127.7, 124.2, 119.9, 109.8, 53.23, 33.96, 29.21, 29.08, 28.97, 27.82, 26.69, 24.65; HRMS (ESI+) *m/z* [M+H] calculated ($C_{16}H_{25}N_4O_2$) 305.1972, observed 305.1984, δ ppm 3.9.

*12-[(1H-1,2,3-benzotriazol-1-yl)amino]dodecanoic acid (**9**).* Synthesized from 12-hydroxydodecanoic acid and **ABT** according to general procedures I, II and III, with respective yields of 22, 55 and 71%. ^{1}H NMR (500 MHz, $CDCl_3$) δ 8.02 (d, *J* = 8.4 Hz, 1H), 7.61 (d, *J* = 8.3, 1H), 7.49 (t, *J* = 8.0 1H), 7.36 (t, *J* = 7.8, 1H), 3.40 (t, *J* = 7.2, 2H), 2.35 (t, *J* = 7.5, 2H), 1.63 (p, *J* = 7.4, 2H), 1.53 (p, *J* = 7.5, 2H), 1.41 (p, *J* = 7.6, 2H), 1.26 (m, 12h); ^{13}C NMR (125 MHz, $CDCl_3$) δ 179.5, 144.3, 132.2, 127.7, 124.2, 119.9, 109.8, 53.27, 34.06, 29.39, 29.32, 29.28, 29.16, 29.02, 27.83, 26.73, 24.70; HRMS (ESI+) *m/z* $[M+H]^+$ calculated ($C_{18}H_{29}N_4O_2$) 333.2285, observed 333.2297, δ ppm 3.6.

CYP4Z1-Mediated Luciferin-Benzyl Ether (Luc-BE) *O*-Debenzylation. To compare Luc-BE (Promega, Madison, Wisconsin) *O*-debenzylation activity between the CYP4Z1-HepG2 (81 pmol CYP4Z1/mg membrane protein) and Vector-HepG2 membrane stocks (Supporting Information: **Method for Membrane Preparation**), metabolic reactions were set up in triplicate on ice and contained 0.6 mg/mL HepG2 membrane protein in 100 mM KPi, pH 7.4, in a final volume of 100 μL. Luc-BE was added to achieve a final concentration of 50 μM and samples were equilibrated at 37 °C for 5 min. NADPH was added for a final concentration of 1mM, or KPi was added for the minus NADPH controls. Metabolic reactions were allowed to proceed for 20 min at 37 °C. To assess the kinetics of CYP4Z1-mediated Luc-BE *O*-debenzylation, metabolic reactions were set up in triplicate on ice and contained 3 pmol of CYP4Z1, in 100 mM KPi, pH

7.4, in a final volume of 100 μL. Luc-BE was added for final concentrations of 1, 5, 10, 25, 50, 75, 100, and 150 μM and the reactions were equilibrated at 37 °C for 5 min. NADPH was added for a final concentration of 1 mM, and metabolism was allowed to proceed for 10 minutes at 37 °C.

Luminescence Assay (General Procedure IV). The CYP4Z1-mediated Luc-BE *O*-debenzylation reactions outlined above, those discussed below to assess inhibition of CYP4Z1 activity, and the other CYP-mediated pro-luciferin metabolism reactions, were quenched (with P450 glo) and assayed as follows: Reactions were transferred from their incubation tubes to white walled 96-well plates containing an equal volume of P450-glo luciferase detection reagent (Promega, Madison, Wisconsin). Beetle luciferin metabolite standards (Promega), prepared in identical matrices, were added at the same time as the metabolic reactions to the plates. After gently mixing and a 20-minute incubation at room temperature, the plates were read on a Biotek Synergy HTX Microplate Reader (Winooski, VT). The luminescence generated (relative light units, RLU) from the calibration luciferin standards was used to generate a standard curve to quantitate the metabolite concentrations in the reactions. These data were subsequently used to determine rates of CYP4Z1 activity and for comparisons between inhibitor and vehicle treated reactions.

CYP4 Isozyme IC_{50}-Shift Experiments. IC_{50}-shift experiments to test inhibition of recombinantly expressed CYP4 isozymes were each performed separately, with duplicate technical replicates, and the experiments were repeated two to three times on separate days. Each metabolic reaction in the experiments contained one of the following: 4 pmol of CYP4Z1 (HepG2 membranes), 1.5 pmol CYP4F8 (HepG2 membranes), 4 pmol of CYP4A11, CYP4F2, CYP4F3a, CYP4F3b, CYP4F12 (Corning Supersomes™, New York, NY). Total protein concentration for all reactions was ~0.20 – 0.25 mg/mL, except for CYP4F8, which was 0.35 mg/mL due to the lower specific content of the enzyme in the HepG2 membrane preparation.

Reactions were set up on ice containing the specific CYP4 isozyme in 100 mM KPi, pH 7.4, in a final volume of 200 μL. All inhibitors were solvated in DMSO to make 200× stocks and added to the reactions to achieve final concentrations spanning 0.001 – 100 μM (**1 – 9** for CYP4Z1), 0.03 – 1000 μM (**ABT** for CYP4Z1), 1 – 3000 μM (**6** for off-target CYP4 isozymes), or 1 – 1000 μM (**7** for off-target CYP4 isozymes). An equal volume of DMSO was added to all vehicle control samples and DMSO concentrations did not exceed 0.5% v/v for all reactions. In order to assess time-dependent inhibition for the inhibitors, half of the metabolic reactions (for each isozyme) included a pre-incubation step plus the cofactor NADPH and the other half a pre-incubation step minus NADPH. The temporal and reagent addition scheme used was as follows: After a 5-min equilibration at 37 °C, NADPH was added from a 50× stock solution for a final concentration of 1 mM to the plus NADPH pre-incubation samples, and an equal volume of buffer to the minus NADPH pre-incubation samples. After a subsequent 30-minute pre-incubation at 37 °C, pro-luciferin probe substrates for each isozyme (detailed below) were added to both sets of pre-incubation reactions from 50× stocks (all at final concentrations ≤ K_m values). Next, NADPH was added to the minus NADPH pre-incubation reactions and an equal volume of buffer to the plus NADPH pre-incubation reactions. The probe substrate reactions were allowed to proceed for 10 minutes at 37 °C and reactions were assayed according to general procedure IV. The pro-luciferins (all from Promega) that were used as CYP4 isozyme probe substrates (concentrations) and the biotransformations that were monitored were as follows: CYP4Z1 Luc-BE (29 μM), CYP4F8 Luc-BE (12 μM), and CYP4F12 Luc-BE (23 μM) *O*-debenzylation; CYP4A11 Luc-4A (80 μM) *O*-demethylation; CYP4F2, CYP4F3a, and CYP4F3b, Luc-4F2/3 (2 μM, due to substrate inhibition kinetics that was observed for all three enzymes, **Figure S7**) *O*-(4-methylthio)-debenzylation. As no metabolite standard for Luc-4A or Luc-4F2/3 was available, enzymatic activity was assessed in a semi-quantitative fashion for isozymes metabolizing these probe substrates. The counter-screening TDI experiment that is presented in **Figure 4** used the

same methods as detailed above except with only a single concentration of 30 μM for inhibitors **2 – 9** and HET0016, as a general CYP4 inhibitor positive control, at 0.5 μM.

Hepatic CYP Isozyme IC_{50}-Shift Experiments. IC_{50}-shift experiments to test Inhibition of hepatic CYP isoforms by **6** and **7** were performed with duplicate technical replicates and experiments were repeated three times on separate days. The assays utilized pooled human liver microsomes (HLM) made up from eight random, individual donor livers, that had been prepared for a previous study[52] and followed a cocktail approach similar to previously published methods.[19,33] The metabolic reactions contained HLM at 0.25 mg/mL total protein, inhibitor **6** or **7** at 1 – 3000 or 1 – 1000 μM, respectively, and used the same setup, timing, and reagent addition scheme as that followed for the CYP4 isozyme IC_{50}-shift experiments. However, after the pre-incubation period, a cocktail of seven selective probe substrates (see below) combined was added from a 50× stock. The CYP isoforms evaluated, substrates (concentrations), and biotransformations were as follows: CYP1A2 phenacetin (100 μM) *O*-deethylation; CYP2B6 bupropion (12 μM) 1'-hydroxylation; CYP2C8 amodiaquine (1 μM) *N*-deethylation; CYP2C9 tolbutamide (100 μM) methyl-hydroxylation; CYP2C19 (*S*)-mephenytoin (50 μM) 4'-hydroxylation; CYP2D6 dextromethorphan (2.5 μM) *O*-demethylation; and CYP3A4/5 midazolam (2.5 μM) 1'-hydroxylation. All probe substrates were used at concentrations ≤ K_m. After probe substrate turnover had proceeded for 10 minutes at 37 °C, reactions were subsequently terminated with an equal volume of ice-cold acetonitrile containing 200 nM of each deuterated internal standard (listed below) and centrifuged at 15,000 × *g* for 10 min. A supernatant aliquot (5 μL) was analyzed by UPLC−MS/MS on a Waters Acquity UPLC connected to a Waters Xevo TQ-S instrument in ESI+ mode, with the following settings: capillary 3.1 kV, source offset 60.0 V, source temperature 150 °C, desolvation temperature 350 °C, cone gas flow 150 L/h, desolvation gas flow 800 L/hour, and collision gas flow 0.15 mL/min. Cone voltage and collision energies varied between analytes and are noted below. Analytes

were separated chromatographically using a Waters HSS T3 column (2.1 × 100 mm, 1.8 μm), starting with 95% mobile phase A (0.1% formic acid in H2O) and 5% mobile phase B (0.1% formic acid in acetonitrile) at a flow rate of 0.3 mL/min. After holding for 1 min, B was increased linearly from 5 to 60% between 1 and 7 min, immediately elevated to 95%, and then held at 95% between 7 and 8.5 min; total run time was 11 min following a 2.5 min equilibration period. The metabolites were detected by multiple reaction monitoring (MRM) with the following transitions, cone voltages (CV), and collision energies (CE): acetaminophen *m/z* 152.2 > 110, CV = 40 V, CE = 20 eV; hydroxybupropion *m/z* 256.1 > 238.1, CV = 32 V, CE = 10 eV; *N*-desethylamodiaquine *m/z* 328.1 > 283, CV = 40 V, CE = 20 eV; hydroxytolbutamide *m/z* 287.1 > 107, CV = 40 V, CE = 20 eV; 4-hydroxymephenytoin *m/z* 235.1 > 150.1, CV = 30 V, CE = 20 eV; dextrorphan *m/z* 258.1 > 157, CV = 40 V, CE = 30 eV; and 1'-hydroxymidazolam *m/z* 342.1 > 203, CV = 40 V, CE = 30 eV. The corresponding isotope-labeled internal standards and MRM transitions were as follows: acetaminophen-d3 *m/z* 155.2 > 111.06, hydroxybupropion-d6 *m/z* 262.2 > 244.2, *N*-desethylamodiaquine-d5 *m/z* 333.1 > 283.1, hydroxytolbutamide-d9 *m/z* 296.1 > 107, 4-hydroxymephenytoin-d3 *m/z* 238.1 > 150.1, dextrorphan-d3 *m/z* 261.2 > 157, and 1'-hydroxymidazolam-d4 *m/z* 346.1 > 203.05. Metabolite standards, using identical matrix and work-up conditions, were used to create standard curves that were utilized in quantitation of the metabolites and subsequent comparison of enzymatic activity between inhibitor and vehicle treated metabolic reactions.

Kinetics of CYP4Z1 Inactivation From 7. Inhibition reactions were set up on ice in triplicate and contained 5 pmol CYP4Z1 in 100 mM KPi, pH 7.4, in a final volume of 100 μL. Inhibitor **7** was added to achieve final concentrations of 0.3, 1, 3, 6, 10, and 20 μM, and DMSO alone was utilized as a vehicle control. After a 5 min equilibration at 37 °C, the reactions were initiated by the addition of NADPH (1 mM final concentration). Aliquots of the inhibition reaction (10 μL) were taken at times 0, 3, 5, 10, 15, and 20 min, diluted 10-fold into a 100 μL probe

substrate reaction containing Luc-BE, at 10 × the determined K_m for CYP4Z1 (290 μM), in 100 mM KPi buffer with 1 mM NADPH. The probe substrate reactions progressed for 10 min at 37 °C and were quenched with an equal volume of ice-cold acetonitrile containing 200 nM Luc-4A as an internal standard and centrifuged at 15,000 × *g* for 10 min. Note: due to the timing constraints of assaying for the kinetics of enzyme inactivation, LC-MS/MS was utilized to detect the luciferin metabolite from CYP4Z1 Luc-BE *O*-debenzylation. A supernatant aliquot (3 μL) was analyzed by UPLC−MS/MS on a Waters Acquity UPLC connected to a Waters Xevo TQ-S instrument in ESI+ mode, with the following settings: capillary 2.8 kV, cone 40.0 V, collision 20.0 V, source offset 60.0 V, source temperature 150 °C, desolvation temperature 350 °C, cone gas flow 150 L/h, desolvation gas flow 800 L/hour, and collision gas flow 0.15 mL/min. Analytes were separated chromatographically using a Waters BEH C18 column (2.1 × 50 mm, 1.7 μm), starting with 95% mobile phase A (0.1% formic acid in H2O) and 5% mobile phase B (0.1% formic acid in acetonitrile) at a flow rate of 0.3 mL/min. After holding for 1 min, B was increased linearly from 5 to 95% between 1 and 4 min and held at 95% between 4 and 6 min; total run time was 8.5 min following a 2.5 min equilibration period. The metabolite luciferin was detected by MRM at *m/z* 281.0 > 234.92 and the internal standard Luc-4A was detected by MRM at *m/z* 289.1 > 201.96. The metabolite luciferin, using identical matrix and work-up conditions, was used to create a standard curve that was utilized in quantitation of the metabolite concentration in the reactions and subsequent comparison of enzymatic activity between inhibitor and vehicle treated metabolic reactions. The natural logarithm of the remaining CYP4Z1 activity after treatment with varying concentrations of **7** was plotted versus pre-incubation time. The resultant differential slopes generated k_{obs} rates, which were then plotted against the concentrations of **7** to allow for the determination of the inactivation parameters K_I and k_{inact}.

Examination of the Effects of Dialysis on CYP4Z1 Inactivation by 7. Inhibition reactions were set up on ice in triplicate and contained 3 pmol CYP4Z1 in 100 mM KPi, pH 7.4,

in a final volume of 100 µL. Inhibitor **7** was added for a final concentration of 3 µM, and DMSO was added to vehicle reactions. After a 5 min equilibration at 37 °C, the reactions were initiated by the addition of NADPH (1 mM final concentration), or KPi buffer only for the minus NADPH samples. The reactions were allowed to proceed for 15 min and then, for the pre-dialysis samples, aliquots (10 µL) were removed and diluted 10-fold into a 100 µL probe substrate reaction containing Luc-BE, at 10 × the determined K_m for CYP4Z1 (290 µM), in 100 mM KPi buffer with 1 mM NADPH. The probe substrate reactions progressed for 10 min at 37 °C and were assayed according to general procedure IV. For the post-dialysis samples (following the 15 min inhibition reaction), the entirety of the reaction was immediately transferred to 10,000 molecular weight cut-off mini dialysis cups (Thermo Scientific Slide-A-Lyzer) suspended in 1 L of 100 mM KPi, pH 7.4, and incubated at 4° C with gentle stirring overnight. The next morning, aliquots were removed, diluted into probe substrate reactions, and assayed as described for the pre-dialysis samples.

Examination of the Effects of Trapping Agents and Reactive Oxygen-Scavenging Enzymes on CYP4Z1 Inactivation by 7. Inhibition reactions were set up on ice in triplicate and contained 3 pmol CYP4Z1 in 100 mM KPi, pH 7.4, in a final volume of 100 µL. Inhibitor **7** was added for a final concentration of 3 µM, and DMSO was added to vehicle reactions. Reduced glutathione, *N*-acetyl-lysine, methoxyamine, *N*-acetyl-cysteine, and semicarbazide were added individually to reactions for final concentrations of 5 mM, and potassium cyanide was added to a reaction for a final concentration of 1 mM. Catalase (CAT) and super oxide dismutase (SOD), from Sigma (St. Louis, MO), were both added to an inhibition reaction together at 80 units each. Both inhibitor **7** and DMSO vehicle reactions were set up for each additive listed above. After a 5 min equilibration at 37 °C, the reactions were initiated by the addition of NADPH (1 mM final concentration) or KPi for the minus NADPH samples. The reactions were allowed to proceed for 15 min at 37 °C, and then aliquots of the inhibition reaction (10 µL) were diluted 10-fold into a

100 µL probe substrate reaction containing Luc-BE, at 10 × the determined K_m for CYP4Z1 (290 µM), in 100 mM KPi buffer with 1 mM NADPH. The probe substrate reactions progressed for 10 min at 37 °C and were assayed according to general procedure IV.

Determination of the Partition Ratio. The number of molecules of **7** metabolized per molecule of CYP4Z1 inactivated, the partition ratio, was estimated from a dilution method. Inhibition reactions were set up on ice in triplicate and contained 5 pmol CYP4Z1 in 100 mM KPi, pH 7.4, in a final volume of 100 µL. Inhibitor **7** was added at 11 different final concentrations spanning 0 to 50 µM. After a 5 min equilibration at 37 °C, the inactivation reactions were initiated by the addition of NADPH (1 mM final concentration). The reactions were allowed to proceed for 45 minutes at 37 °C to allow for maximal inactivation, and then aliquots of the inhibition reaction (10 µL) were diluted 10-fold into a 100 µL probe substrate reaction containing Luc-BE, at 10 × the determined K_m for CYP4Z1 (290 µM), in 100 mM KPi buffer with 1 mM NADPH. The probe substrate reactions progressed for 10 min at 37 °C and were assayed according to general procedure IV. The percentage of remaining CYP4Z1 activity was plotted versus the molar ratio of [**7**]/[CYP4Z1]. Extrapolation of the initial linear portion to the *x*-intercept generated the turnover number; the partition number was then calculated as the turnover number minus 1.

Inhibition of CYP4Z1-Mediated AA Metabolism in T47D Cells by 7. T47D cells were modified to express CYP4Z1 (CYP4Z1-T47D), or a control vector (Vector-T47D), in a similar fashion to the HepG2 cell lines. A schematic outline of the lentiviral vector system has been provided in the Supporting Information (**Figure S1A**). Western blot analysis was performed as previously described.[8] The stably transduced cell lines were grown in tissue culture media consisting of RPMI-1640, 1%Glutamine, 10% FBS, and 0.01 mg/ml Insulin and selected with puromycin treatment (2 µg/mL) over a 4-day period to ensure homogenous transduction profiles. Both CYP4Z1- and Vector-T47D cell lines were seeded into 6-well tissue culture-

treated plates at 2.5×10^5 cells/mL in a volume of 2 mL/well. The CYP4Z1-T47D cells were then dosed with inhibitor **7** to achieve final concentrations of 1 and 3 μM from 1000× DMSO stocks, or DMSO vehicle was added (plus 24-hour pre-incubation samples); Vector-T47D cells were dosed with DMSO. The cells were then placed in a tissue culture incubator at 37° C. After 24 hours, AA was added to all wells for a final concentration of 50 μM from a 400× concentrated stock solvated in degassed ethanol. Inhibitor **7** was then added to the CYP4Z1-T47D cells, which had not been dosed the day prior (minus 24-hour pre-incubation samples), at 1 and 3 μM, or DMSO vehicle was added; Vector-T47D cells were dosed with DMSO. Cells were placed back into the tissue culture incubator for 2 hours to allow for CYP4Z1-mediated AA oxidation. Following this incubation period, media was collected from each well and 0.5 mL H_2O was added to the wells which were then incubated at room temperature for 1 minute. Subsequently, 1 mL of a 1:1 mixture of acetonitrile and methanol was added to each well and cells were scraped to remove them from the tissue culture dish. The aqueous and organic mixture was pooled with the respective media collections and a further 1 mL of the acetonitrile/methanol mixture was added to rinse the wells of any remaining cells and/or extracted analytes. The combined aqueous and organic fractions were then subjected to a previously described workup[8] and a supernatant aliquot (10 μL) was analyzed by UPLC−MS/MS on a Waters Acquity UPLC connected to a Waters Xevo TQ-S instrument in ESI- mode using settings, chromatography gradient, and column as previously described by McDonald et al.[8] The oxidative AA metabolites 14,15-DiHET, 19-HETE, 20-HETE, and 14,15-EET were detected by MRM at *m/z* 337.10 > 207.00, 319.1 > 231, 319 > 245, and 319.1 > 219, respectively. The deuterated internal standards 14,15-DiHET-d11, 20-HETE-d6, and 14,15-EET-d11 were detected by MRM at *m/z* 348.30 > 207.20, 325.10 > 281.10, and 330.20 > 218.80, respectively. Relative inhibition of AA metabolite formation was determined by comparing the peak area ratios of the analytes divided by their respective deuterated internal standards from cells treated with **7** compared to vehicle,

at the various timepoints and conditions noted above. As no deuterated internal standard for 19-HETE is available, 20-HETE-d6 was utilized as the internal standard for this AA metabolite. The entire experiment was repeated under similar conditions and yielded comparable results (data not shown).

Data Analysis. GraphPad Prism 7.00 (San Diego, CA) was used for graphing all results, to estimate all kinetic parameters (K_m, V_{max}, K_I, and k_{inact}), and to determine the half maximal inhibitory concentration (IC_{50}) values. IC_{50} values from each individual experiment were averaged and standard deviations calculated. Mass spectral analysis was performed with Waters MassLynx V4.1 and Thermo Xcalibur V2.0. ^{1}H and ^{13}C NMR spectral analysis was performed with Bruker TopSpin V4.0.7.

Associated Content

Supporting Information

CYP4Z1 expression systems; Method for Membrane Preparation; IC_{50} and shifted-IC_{50} determination for inhibition of CYP4Z1 by **1** – **9**; IC_{50} and shifted-IC_{50} determination for inhibition of CYP4 isoforms by **6**; IC_{50} and shifted-IC_{50} determination for inhibition of CYP4 isoforms by **7**; IC_{50} and shifted-IC_{50} determination for inhibition of hepatic CYP isoforms by **6**; IC_{50} and shifted-IC_{50} determination for inhibition of hepatic CYP isoforms by **7**; Luc-4F2/3 metabolism kinetics for CYP4F2, CYP4F3a, and CYP4F3b; Analysis of CYP4F8 metabolism of pro-luciferins; Internal validation of HLM cocktail inhibition assay; Inhibition of CYP4Z1-mediated AA Metabolism by **7** in HepG2 Membranes; Inhibition of CYP4Z1 in HepG2 Cells and HepG2, T47D Cell Viability; ^{1}H and ^{13}C NMR Spectra; Molecular Formula Strings Spreadsheet

Acknowledgements

We thank Dale Whittington and J. Scott Edgar for assistance in the University of Washington, Department of Medicinal Chemistry, Mass Spectrometry Center. We also thank Adrienne Roehrich for assistance in the University of Washington, Department of Chemistry, NMR Facility. Lastly, we thank Kent Kunze for helpful discussions regarding mechanism-based inactivation of CYP450s.

Abbreviations

CYP4Z1, cytochrome P450 4Z1; KPi, potassium phosphate buffer; **ABT**, 1-aminobenzotriazole; Luc-BE, luciferin-benzyl ether; NADPH, Reduced β-nicotinamide-adenine dinucleotide phosphate; MBI, mechanism-based inhibitor; TDI, time-dependent inhibition; IC_{50}, half maximal inhibitory concentration; AA, arachidonic acid; LA, lauric acid; 14,15-EET, 14,15-epoxyeicosatrienoic acid; 20-HETE, 20-hydroxyeicosatetraenoic acid; PUFA, polyunsaturated fatty acid; CAT, catalase; SOD, super oxide dismutase; GSH, glutathione; NAL, *N*-acetyl lysine; $MeONH_2$, methoxyamine; NAC, *N*-acetyl cysteine; KCN, potassium cyanide

References

(1) Ortiz de Montellano, P.R. Cytochrome P450: Structure, Mechanism, and Biochemistry. New York, NY: *Kluwer Academic/Plenum Publishers*; **2005**.

(2) Rieger, M. A.; Ebner, R.; Bell, D. R.; Kiessling, A.; Rohayem, J.; Schmitz, M.; Temme, A.; Rieber, E. P.; Weigle, B. Identification of a novel mammary-restricted cytochrome P450, CYP4Z1, with overexpression in breast carcinoma. *Cancer Res* **2004,** 64, 2357-2364.

(3) Yu, W.; Chai, H.; Li, Y.; Zhao, H.; Xie, X.; Zheng, H.; Wang, C.; Wang, X.; Yang, G.; Cai, X.; Falck, J. R.; Yang, J. Increased expression of CYP4Z1 promotes tumor angiogenesis and growth in human breast cancer. *Toxicol Appl Pharmacol* **2012,** 264, 73-83.

(4) Edson, K. Z.; Rettie, A. E. CYP4 enzymes as potential drug targets: focus on enzyme multiplicity, inducers and inhibitors, and therapeutic modulation of 20-hydroxyeicosatetraenoic acid (20-HETE) synthase and fatty acid omega-hydroxylase activities. *Curr Top Med Chem* **2013,** 13, 1429-1440.

(5) Johnson, A. L.; Edson, K. Z.; Totah, R. A.; Rettie, A. E. Cytochrome P450 omega-hydroxylases in inflammation and cancer. *Adv Pharmacol* **2015,** 74, 223-262.

(6) Luo, J.; Feng, X. X.; Luo, C.; Wang, Y.; Li, D.; Shu, Y.; Wang, S. S.; Qin, J.; Li, Y. C.; Zou, J. M.; Tian, D. A.; Zhang, G. M.; Feng, Z. H. 14,15-EET induces the infiltration and tumor-promoting function of neutrophils to trigger the growth of minimal dormant metastases. *Oncotarget* **2016,** 7, 43324-43336.

(7) Panigrahy, D.; Greene, E. R.; Pozzi, A.; Wang, D. W.; Zeldin, D. C. EET signaling in cancer. *Cancer Metastasis Rev* **2011,** 30, 525-540.

(8) McDonald, M. G.; Ray, S.; Amorosi, C. J.; Sitko, K. A.; Kowalski, J. P.; Paco, L.; Nath, A.; Gallis, B.; Totah, R. A.; Dunham, M. J.; Fowler, D. M.; Rettie, A. E. Expression and functional characterization of breast cancer-associated cytochrome P450 4Z1 in saccharomyces cerevisiae. *Drug Metab Dispos* **2017,** 45, 1364-1371.

(9) World Cancer Research Fund. https://www.wcrf.org/dietandcancer/cancer-trends/breast-cancer-statistics (accessed October 2019)

(10) Capper, C. P.; Rae, J. M.; Auchus, R. J. The metabolism, analysis, and targeting of steroid hormones in breast and prostate cancer. *Horm Cancer* **2016,** 7, 149-164.

(11) Bruno, R. D.; Njar, V. C. Targeting cytochrome P450 enzymes: a new approach in anti-cancer drug development. *Bioorg Med Chem* **2007,** 15, 5047-5060.

(12) Westerink, W. M.; Schoonen, W. G. Cytochrome P450 enzyme levels in HepG2 cells and cryopreserved primary human hepatocytes and their induction in HepG2 cells. *Toxicol In Vitro* **2007,** 21, 1581-1591.

(13) Schulz, C.; Kammerer, S.; Küpper, J. H. NADPH-cytochrome P450 reductase expression and enzymatic activity in primary-like human hepatocytes and HepG2 cells for in vitro biotransformation studies. *Clin Hemorheol Microcirc* **2019,** 73, 249-260.

(14) Guengerich, F. P.; Martin, M. V.; Sohl, C. D.; Cheng, Q. Measurement of cytochrome P450 and NADPH-cytochrome P450 reductase. *Nat Protoc* **2009,** 4, 1245-1251.

(15) Yan, Q.; Machalz, D.; Zollner, A.; Sorensen, E. J.; Wolber, G.; Bureik, M. Efficient substrate screening and inhibitor testing of human CYP4Z1 using permeabilized recombinant fission yeast. *Biochem Pharmacol* **2017,** 146, 174-187.

(16) Promega P450-Glo. https://www.promega.com/resources/protocols/technical-bulletins/101/p450-glo-assays-protocol/ (accessed October 2019)

(17) Parkinson, A.; Kazmi, F.; Buckley, D. B.; Yerino, P.; Paris, B. L.; Holsapple, J.; Toren, P.; Otradovec, S. M.; Ogilvie, B. W. An evaluation of the dilution method for identifying metabolism-dependent inhibitors of cytochrome P450 enzymes. *Drug Metab Dispos* **2011,** 39, 1370-1387.

(18) Henne, K. R.; Tran, T. B.; VandenBrink, B. M.; Rock, D. A.; Aidasani, D. K.; Subramanian, R.; Mason, A. K.; Stresser, D. M.; Teffera, Y.; Wong, S. G.; Johnson, M. G.; Chen, X.; Tonn, G. R.; Wong, B. K. Sequential metabolism of AMG 487, a novel CXCR3 antagonist, results in formation of quinone reactive metabolites that covalently modify CYP3A4 Cys239 and cause time-dependent inhibition of the enzyme. *Drug Metab Dispos* **2012,** 40, 1429-1440.

(19) Kozakai, K.; Yamada, Y.; Oshikata, M.; Kawase, T.; Suzuki, E.; Haramaki, Y.; Taniguchi, H. Cocktail-substrate approach-based high-throughput assay for evaluation of direct and time-dependent inhibition of multiple cytochrome P450 isoforms. *Drug Metab Pharmacokinet* **2014,** 29, 198-207.

(20) Grimm, S. W.; Einolf, H. J.; Hall, S. D.; He, K.; Lim, H. K.; Ling, K. H.; Lu, C.; Nomeir, A. A.; Seibert, E.; Skordos, K. W.; Tonn, G. R.; Van Horn, R.; Wang, R. W.; Wong, Y. N.; Yang, T. J.; Obach, R. S. The conduct of in vitro studies to address time-dependent inhibition of drug-metabolizing enzymes: a perspective of the pharmaceutical research and manufacturers of America. *Drug Metab Dispos* **2009,** 37, 1355-1370.

(21) Hollenberg, P. F.; Kent, U. M.; Bumpus, N. N. Mechanism-based inactivation of human cytochromes p450s: experimental characterization, reactive intermediates, and clinical implications. *Chem Res Toxicol* **2008,** 21, 189-205.

(22) Emoto, C.; Murase, S.; Sawada, Y.; Jones, B. C.; Iwasaki, K. In vitro inhibitory effect of 1-aminobenzotriazole on drug oxidations catalyzed by human cytochrome P450 enzymes: a comparison with SKF-525A and ketoconazole. *Drug Metab Pharmacokinet* **2003,** 18, 287-295.

(23) Ortiz de Montellano, P. R. 1-Aminobenzotriazole: A Mechanism-Based Cytochrome P450 Inhibitor and Probe of Cytochrome P450 Biology. *Med Chem (Los Angeles)* **2018,** 8, 3.

(24) Mathews, J. M.; Bend, J. R. N-alkylaminobenzotriazoles as isozyme-selective suicide inhibitors of rabbit pulmonary microsomal cytochrome P-450. *Mol Pharmacol* **1986,** 30, 25-32.

(25) Mathews, J. M.; Bend, J. R. N-aralkyl derivatives of 1-aminobenzotriazole as potent isozyme-selective mechanism-based inhibitors of rabbit pulmonary cytochrome P450 in vivo. *J Pharmacol Exp Ther* **1993,** 265, 281-285.

(26) Woodcroft, K. J.; Szczepan, E. W.; Knickle, L. C.; Bend, J. R. Three N-aralkylated derivatives of 1-aminobenzotriazole as potent and isozyme-selective, mechanism-based inhibitors of guinea pig pulmonary cytochrome P-450 in vitro. *Drug Metab Dispos* **1990,** 18, 1031-1037.

(27) Hsu, M. H.; Baer, B. R.; Rettie, A. E.; Johnson, E. F. The crystal structure of cytochrome P450 4B1 (CYP4B1) monooxygenase complexed with octane discloses several structural adaptations for omega-hydroxylation. *J Biol Chem* **2017,** 292, 5610-5621.

(28) Miyata, N.; Taniguchi, K.; Seki, T.; Ishimoto, T.; Sato-Watanabe, M.; Yasuda, Y.; Doi, M.; Kametani, S.; Tomishima, Y.; Ueki, T.; Sato, M.; Kameo, K. HET0016, a potent and selective inhibitor of 20-HETE synthesizing enzyme. *Br J Pharmacol* **2001,** 133, 325-329.

(29) Nakamura, T.; Sato, M.; Kakinuma, H.; Miyata, N.; Taniguchi, K.; Bando, K.; Koda, A.; Kameo, K. Pyrazole and isoxazole derivatives as new, potent, and selective 20-hydroxy-5,8,11,14-eicosatetraenoic acid synthase inhibitors. *J Med Chem* **2003,** 46, 5416-5427.

(30) Bylund, J.; Bylund, M.; Oliw, E. H. cDna cloning and expression of CYP4F12, a novel human cytochrome P450. *Biochem Biophys Res Commun* **2001,** 280, 892-897.

(31) Bylund, J.; Hidestrand, M.; Ingelman-Sundberg, M.; Oliw, E. H. Identification of CYP4F8 in human seminal vesicles as a prominent 19-hydroxylase of prostaglandin endoperoxides. *J Biol Chem* **2000,** 275, 21844-21849.

(32) U.S. Food & Drug Administration. https://www.fda.gov/drugs/drug-interactions-labeling/drug-development-and-drug-interactions-table-substrates-inhibitors-and-inducers (accessed October 2019)

(33) Li, G.; Huang, K.; Nikolic, D.; van Breemen, R. B. High-throughput cytochrome P450 cocktail inhibition assay for assessing drug-drug and drug-botanical interactions. *Drug Metab Dispos* **2015,** 43, 1670-1678.

(34) Fer, M.; Dreano, Y.; Lucas, D.; Corcos, L.; Salaun, J. P.; Berthou, F.; Amet, Y. Metabolism of eicosapentaenoic and docosahexaenoic acids by recombinant human cytochromes P450. *Arch Biochem Biophys* **2008,** 471, 116-125.

(35) Kaspera, R.; Totah, R. A. Epoxyeicosatrienoic acids: formation, metabolism and potential role in tissue physiology and pathophysiology. *Expert Opin Drug Metab Toxicol* **2009,** 5, 757-771.

(36) Mitra, R.; Guo, Z.; Milani, M.; Mesaros, C.; Rodriguez, M.; Nguyen, J.; Luo, X.; Clarke, D.; Lamba, J.; Schuetz, E.; Donner, D. B.; Puli, N.; Falck, J. R.; Capdevila, J.; Gupta, K.; Blair, I. A.; Potter, D. A. CYP3A4 mediates growth of estrogen receptor-positive breast cancer cells in part by inducing nuclear translocation of phospho-Stat3 through biosynthesis of (+/-)-14,15-epoxyeicosatrienoic acid (EET). *J Biol Chem* **2011,** 286, 17543-17559.

(37) Johnson, D. S.; Weerapana, E.; Cravatt, B. F. Strategies for discovering and derisking covalent, irreversible enzyme inhibitors. *Future Med Chem* **2010,** 2, 949-964.

(38) Brueggemeier, R. W.; Hackett, J. C.; Diaz-Cruz, E. S. Aromatase inhibitors in the treatment of breast cancer. *Endocr Rev* **2005,** 26, 331-345.

(39) Silverman, R. B., Mechanism-Based Enzyme Inactivation: Chemistry and Enzymology. Boca Raton, FL: *CRC Press*; **1988.**

(40) Giudici, D.; Ornati, G.; Briatico, G.; Buzzetti, F.; Lombardi, P.; di Salle, E. 6-Methylenandrosta-1,4-diene-3,17-dione (FCE 24304): a new irreversible aromatase inhibitor. *J Steroid Biochem* **1988,** 30, 391-394.

(41) Sodhi, J. K.; Delarosa, E. M.; Halladay, J. S.; Driscoll, J. P.; Mulder, T.; Dansette, P. M.; Khojasteh, S. C. Inhibitory effects of trapping agents of sulfur drug reactive intermediates against major human cytochrome P450 isoforms. *Int J Mol Sci* **2017,** 18, 1553.

(42) Wang, E.; Walsh, C. Suicide substrates for the alanine racemase of Escherichia coli B. *Biochemistry* **1978,** 17, 1313-1321.

(43) Lim, H. K.; Duczak, N., Jr.; Brougham, L.; Elliot, M.; Patel, K.; Chan, K. Automated screening with confirmation of mechanism-based inactivation of CYP3A4, CYP2C9, CYP2C19, CYP2D6, and CYP1A2 in pooled human liver microsomes. *Drug Metab Dispos* **2005,** 33, 1211-1219.

(44) Holliday, D. L.; Speirs, V. Choosing the right cell line for breast cancer research. *Breast Cancer Res* **2011,** 13, 215.

(45) Nishikiori, M.; Iizuka, H.; Ichiba, H.; Sadamoto, K.; Fukushima, T. Determination of free fatty acids in human serum by HPLC with fluorescence detection. *J Chromatogr Sci* **2015,** 53, 537-541.

(46) Wang, W.; Qin, S.; Li, L.; Chen, X.; Wang, Q.; Wei, J. An optimized high throughput clean-up method using mixed-mode SPE plate for the analysis of free arachidonic acid in plasma by LC-MS/MS. *Int J Anal Chem* **2015,** 2015, 374819.

(47) Decker, M.; Adamska, M.; Cronin, A.; Di Giallonardo, F.; Burgener, J.; Marowsky, A.; Falck, J. R.; Morisseau, C.; Hammock, B. D.; Gruzdev, A.; Zeldin, D. C.; Arand, M. EH3 (ABHD9): the first member of a new epoxide hydrolase family with high activity for fatty acid epoxides. *J Lipid Res* **2012,** 53, 2038-2045.

(48) Vogel, A.I.; Tatchell, A.R.; Furnis, B.S.; Hannaford, A.J.; Smith, P.W.G. Vogel's Textbook of Practical Organic Chemistry, 5th Edition. New York, NY: *John Wiley & Sons*; **1996.**

(49) Wiek, C.; Schmidt, E. M.; Roellecke, K.; Freund, M.; Nakano, M.; Kelly, E. J.; Kaisers, W.; Yarov-Yarovoy, V.; Kramm, C. M.; Rettie, A. E.; Hanenberg, H. Identification of amino acid determinants in CYP4B1 for optimal catalytic processing of 4-ipomeanol. *Biochem J* **2015,** 465, 103-14.

(50) Roellecke, K.; Virts, E. L.; Einholz, R.; Edson, K. Z.; Altvater, B.; Rossig, C.; von Laer, D.; Scheckenbach, K.; Wagenmann, M.; Reinhardt, D.; Kramm, C. M.; Rettie, A. E.; Wiek, C.; Hanenberg, H. Optimized human CYP4B1 in combination with the alkylator prodrug 4-ipomeanol serves as a novel suicide gene system for adoptive T-cell therapies. *Gene Ther* **2016**, 23, 615-626.

(51) Kowalski, J. P.; McDonald, M. G.; Whittington, D.; Guttman, M.; Scian, M.; Girhard, M.; Hanenberg, H.; Wiek, C.; Rettie, A. E. Structure-activity relationships for CYP4B1 bioactivation of 4-ipomeanol congeners: Direct correlation between cytotoxicity and trapped reactive intermediates. *Chem Res Toxicol* **2019,** 32, 2488-2498.

(52) McDonald, M. G.; Au, N. T.; Rettie, A. E. P450-Based drug-drug interactions of amiodarone and its metabolites: Diversity of inhibitory mechanisms. *Drug Metab Dispos* **2015,** 43, 1661-1669.

(53) Kent, U. M.; Bend, J. R.; Chamberlin, B. A.; Gage, D. A.; Hollenberg, P. F. Mechanism-based inactivation of cytochrome P450 2B1 by N-benzyl-1-aminobenzotriazole. *Chem Res Toxicol* **1997,** 10, 600-608.

(54) Zollner, A.; Dragan, C. A.; Pistorius, D.; Muller, R.; Bode, H. B.; Peters, F. T.; Maurer, H. H.; Bureik, M. Human CYP4Z1 catalyzes the in-chain hydroxylation of lauric acid and myristic acid. *Biol Chem* **2009,** 390, 313-317.

(55) Savas, U.; Hsu, M.-H.; Griffin, K. J.; Bell, D. R.; Johnson, E. F. Conditional regulation of the human CYP4X1 and CYP4Z1 genes. *Archives of biochemistry and biophysics* **2005,** 436, 377-385.

(56) Yang, X.; Hutter, M.; Goh, W. W. B.; Bureik, M. CYP4Z1 - A human cytochrome P450 enzyme that might hold the key to curing breast cancer. *Current pharmaceutical design* **2017,** 23, 2060-2064.

(57) Murray, G. I.; Patimalla, S.; Stewart, K. N.; Miller, I. D.; Heys, S. D. Profiling the expression of cytochrome P450 in breast cancer. *Histopathology* **2010,** 57, 202-211.

(58) Radvanyi L.; Singh-Sandhu D.; Gallichan S.; Lovitt C.; Pedyczak A.; Mallo G.; Gish K.; Kwok K.; Hanna W.; Zubovits J.; Armes J.; Venter D.; Hakimi J.; Shortreed J.; Donovan M.; Parrington M.; Dunn P.; Oomen R.; Tartaglia J.; Berinstein NL.; The gene

associated with trichorhinophalangeal syndrome in humans is overexpressed in breast cancer. *Proc Natl Acad Sci U S A*. **2005**, 102, 11005-11010.

(59) Li Y.; Steppi A.; Zhou Y.; Mao F.; Miller P.C.; He M.M.; Zhao T.; Sun Q.; Zhang J. Tumoral expression of drug and xenobiotic metabolizing enzymes in breast cancer patients of different ethnicities with implications to personalized medicine*. Sci Rep*. **2017,** 7(1):4747.

(60) Al-Esawi N. S. E.; Geeran A. R. M.; Alajeely M. H. J.; Al-Isawi A. O. J. Expression of CYT4Z1 in breast carcinoma; Correlating with clinicopathological parameters. *Biomed Pharmacol J* **2020**, 13(1).

Figures

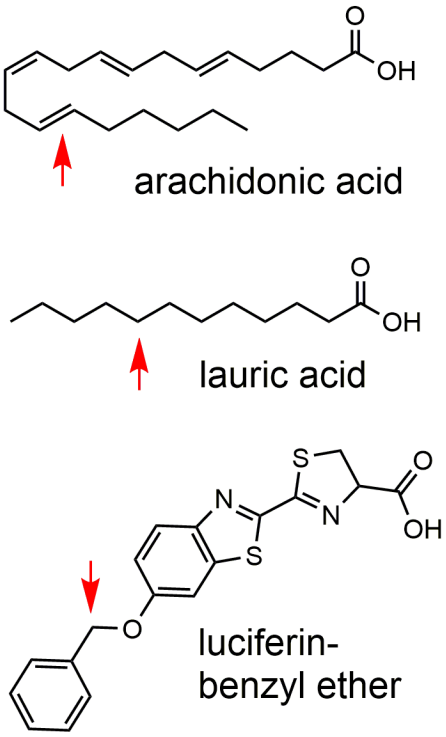

Figure 1. CYP4Z1 metabolizes substrates internally. The primary oxidation positions for substrates arachidonic acid (AA), lauric acid (LA), and luciferin-benzyl ether (Luc-BE) are denoted by the red arrows, generating products 14,15-epoxyeicosatrienoic acid (14,15-EET), 8-hydroxy LA, and luciferin (*via* *O*-dealkylation), respectively.[8,15,54]

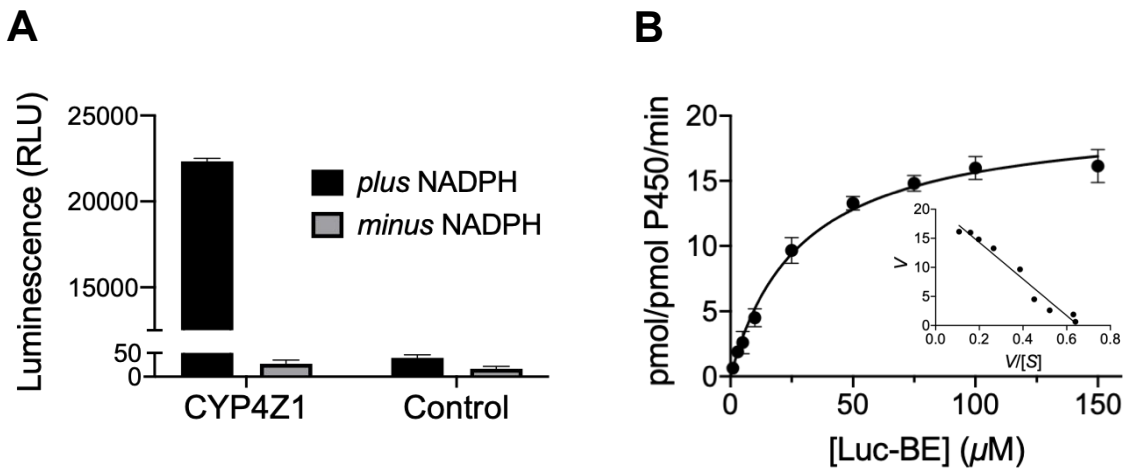

Figure 2. Probe substrate Luc-BE metabolism in the HepG2 membranes is both CYP4Z1- and NADPH-dependent (**A**)**.** CYP4Z1-HepG2 membrane metabolism of Luc-BE displays Michaelis-Menten kinetics at the substrate concentrations tested, with a K_m = 29 μM and a V_{max} = 20 pmol/pmol CYP4Z1/min; the Eadie-Hofstee plot (inset) shows apparent linearity (**B**)**.** Shown is the average ± SD from at least three replicates.

Scheme 1. Synthesis of ABT-Analogs[a]

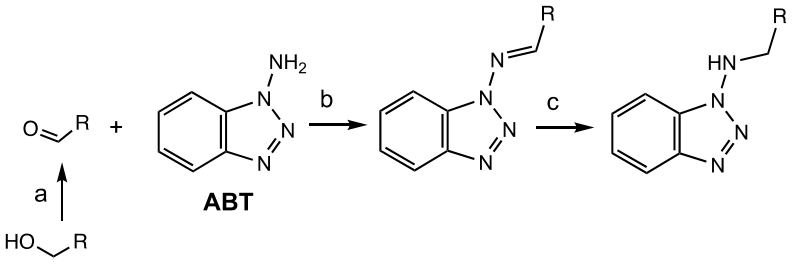

ID	R =
1	propyl
2	pentyl
3	heptyl
4	nonyl
5	undecyl
6	pentanoic acid
7	heptanoic acid
8	nonanoic acid
9	undecanoic acid

[a]Reagents and conditions: (a) celite, PCC, CH_2Cl_2, RT, 1 h, 21-25%, (analogs **6-9**); (b) acetic acid, RT, 18 h, 43-89%; (c) $NaBH_4$, CH_2Cl_2, MeOH, RT, 2 h, 56-84%

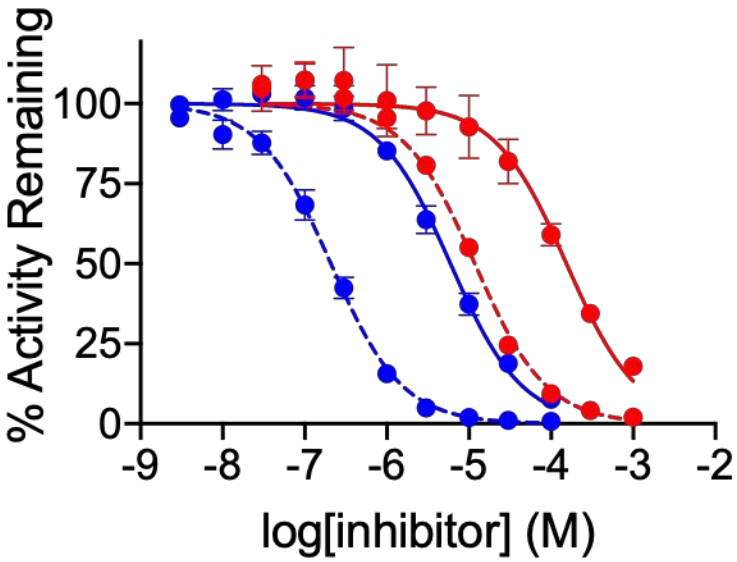

Figure 3. Time-dependent inhibition of CYP4Z1-mediated Luc-BE *O*-debenzylation by **ABT** (red) and inhibitor **7** (blue). Shown is percent activity remaining versus inhibitor concentration, with (dashed lines) and without (solid lines) the presence of NADPH in a pre-incubation step. The ABT-analog **7** exhibited gains in affinity and rate of enzyme inactivation for CYP4Z1 compared to the parent compound. IC_{50} values are reported in **Table 1**. Shown is the average ± SD from three independent experiments.

Table 1. IC_{50} and Shifted-IC_{50} Values for the Inhibition of CYP4Z1-Mediated Luc-BE *O*-debenzylation by ABT and Analogs

Inhibitor	IC_{50} ± SD (μM)	Shifted-IC_{50} ± SD (μM)	Shift Ratio[a]
ABT	154 ± 23	12 ± 0.8	13
1	19 ± 2.6	0.7 ± 0.06	27
2	2.9 ± 0.1	0.1 ± 0.01	30
3	4.9 ± 0.3	0.4 ± 0.05	13
4	12 ± 1.6	0.5 ± 0.05	24
5	46 ± 10	1.4 ± 0.4	32
6	41 ± 2.4	1.7 ± 0.06	24
7	5.9 ± 0.9	0.2 ± 0.04	30
8	4.5 ± 0.4	0.2 ± 0.02	23
9	7.2 ± 0.5	0.3 ± 0.02	24

[a] IC_{50} / Shifted-IC_{50}

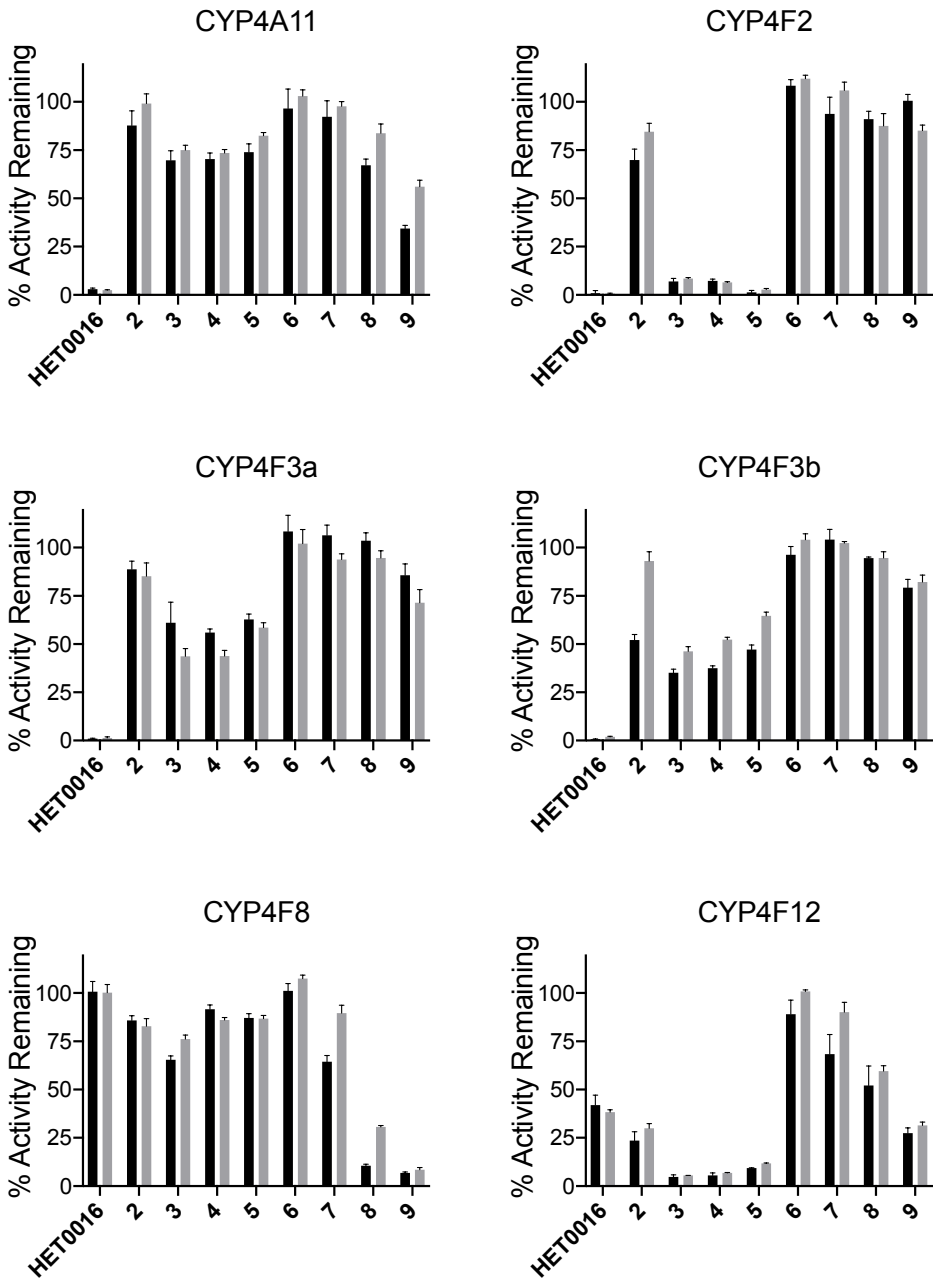

Figure 4. Time-dependent inhibition of CYP4A11-mediated Luc-4A *O*-demethylation, CYP4F2-, CYP4F3a-, CYP4F3b-mediated Luc-4F2/3 *O*-(4-methylthio)-debenzylation, and CYP4F8-, CYP4F12-mediated Luc-BE *O*-debenzylation by ABT-analogs screened at 30 μM. The pan-CYP4 inhibitor HET0016 was dosed at 0.5 μM as an inhibition control. All probe substrates were used at concentrations ≤ K_m. All enzymes were recombinantly expressed in insect cells (Supersomes™), except for CYP4F8 which was recombinantly expressed in HepG2 cells. The black and grey bars show the percent activity remaining when the inhibitor was pre-incubated for 30 minutes with enzyme plus and minus NADPH, respectively. Shown is the average ± SD from three replicates.

Table 2. IC_{50} and Shifted-IC_{50} Values for Inhibition of CYP4-Mediated Pro-Luciferin Metabolism by Inhibitors 6 and 7

CYP	Inhibitor	IC_{50} ± SD (μM)	Shifted-IC_{50} ± SD (μM)	Shift Ratio[a]	Specificity Ratio[b]	TDI Specificity Ratio[c]
4A11	**6**	1330 ± 134	455 ± 20	2.9	32	268
	7	282 ± 15	179 ± 51	1.6	48	895
4F2	**6**	1130 ± 114	647 ± 83	1.7	28	381
	7	212 ± 15	221 ± 36	1.0	36	1105
4F3a	**6**	1240 ± 40	1370 ± 198	0.9	30	808
	7	264 ± 31	447 ± 75	0.6	45	2235
4F3b	**6**	1520 ± 191	1690 ± 185	0.9	37	991
	7	187 ± 6	213 ± 46	0.9	32	1065
4F8	**6**	1180 ± 137	778 ± 53	1.5	29	458
	7	167 ± 23	57 ± 13	2.9	28	285
4F12	**6**	380 ± 39	233 ± 11	1.6	9	137
	7	91 ± 17	46 ± 8	2.0	15	230

[a] IC_{50} / Shifted-IC_{50}

[b] Off-target CYP IC_{50} / CYP4Z1 IC_{50}

[c] Off-target CYP Shifted-IC_{50} / CYP4Z1 Shifted-IC_{50}

Table 3. IC_{50} and Shifted-IC_{50}Values for Inhibition of Hepatic CYP-Mediated Substrate Cocktail Metabolism by Inhibitors 6 and 7

CYP	Inhibitor	IC_{50} ± SD (μM)	Shifted-IC_{50} ± SD (μM)	Shift Ratio[a]	Specificity Ratio[b]	TDI Specificity Ratio[c]
1A2	**6**	2790 ± 272	228 ± 18	12.2	68	134
	7	614 ± 117	55 ± 8	11.2	104	275
2B6	**6**	923 ± 152	258 ± 28	3.6	23	152
	7	257 ± 68	62 ± 21	4.1	44	310
2C8	**6**	2310 ± 71	954 ± 31	2.4	56	561
	7	306 ± 44	84 ± 16	3.6	52	420
2C9	**6**	>3000	1940 ± 56	>1.5	>73	1141
	7	343 ± 88	330 ± 41	1.0	58	1650
2C19	**6**	>3000	1640 ± 189	>1.8	>73	965
	7	759 ± 138	246 ± 62	3.1	129	1230
2D6	**6**	2850 ± 404	1710 ± 107	1.7	70	1006
	7	826 ± 177	299 ± 86	2.8	140	1495
3A4/5	**6**	1310 ± 172	766 ± 29	1.7	32	451
	7	244 ± 8	128 ± 10	1.9	41	640

[a] IC_{50} / Shifted-IC_{50}

[b] Off-target CYP IC_{50} / CYP4Z1 IC_{50}

[c] Off-target CYP Shifted-IC_{50} / CYP4Z1 Shifted-IC_{50}

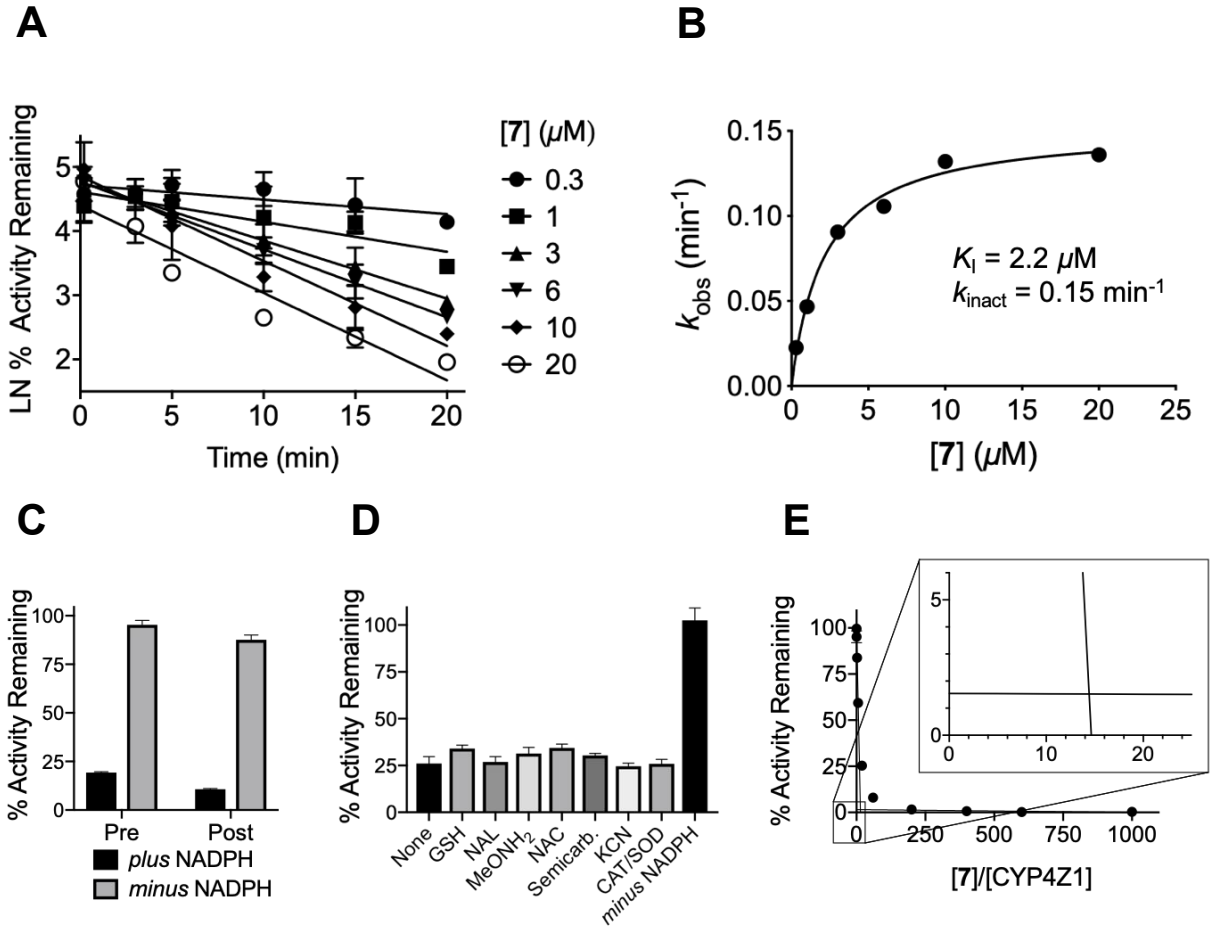

Figure 5. Characterization of mechanism-based inactivation of CYP4Z1 by **7**. Time- and concentration-dependent loss of CYP4Z1-mediated Luc-BE *O*-debenzylation activity from treatment with **7**, K_I = 2.2 μM, k_{inact} = 0.15 min^{-1} (**A, B**). The percent of CYP4Z1 activity remaining when inhibitor **7** was pre-incubated with enzyme plus (black bars) and minus (grey bars) NADPH was assessed both prior to (Pre) and after (Post) overnight dialysis. The TDI of CYP4Z1 was not affected by this dialysis step (**C**). The percent of CYP4Z1 activity remaining when inhibitor **7** was pre-incubated with enzyme plus NADPH was assessed with the following nucleophilic additives: glutathione (GSH), *N*-acetyl-lysine (NAL), methoxyamine ($MeONH_2$), *N*-acetyl-cysteine (NAC), and semicarbazide (semicarb.) at 5 mM and potassium cyanide (KCN) at 1 mM. Inclusion of these trapping agents did not significantly abrogate TDI of CYP4Z1 by **7**. Similarly, addition of the reactive oxygen-scavenging enzymes catalase (CAT) and superoxide dismutase (SOD) did not affect TDI of CYP4Z1 by **7** (**D**). In both (**C**) and (**D**) the minus NADPH sample controls exhibit cofactor dependency for the bioactivation reaction. A plot of the percent of CYP4Z1 activity, when inhibitor **7** was pre-incubated with enzyme plus NADPH, versus the concentration ratio of **7**/CYP4Z1 was used to determine the number of inactivator molecules converted and released as a product relative to each inactivation event. Extrapolation of the initial linear portion of the plot to the x-intercept (inset) shows a turnover number of 15, resulting in a partition ratio of ~14 (**E**)**.** For all assays, shown is the average ± SD from three replicates.

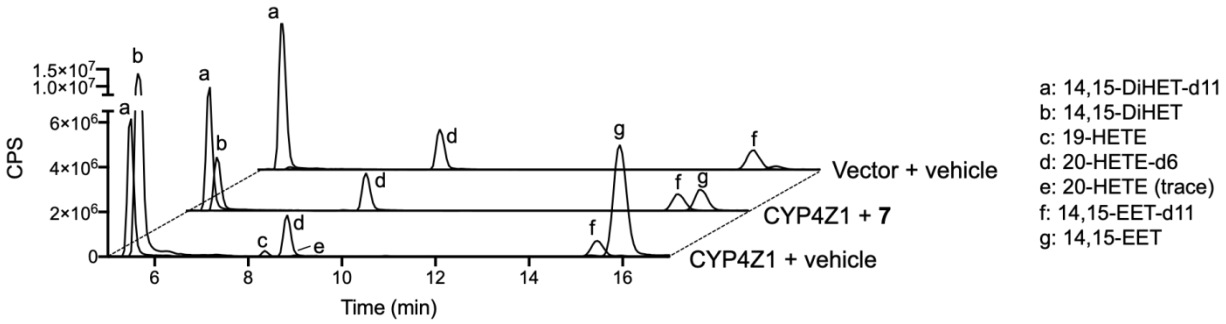

Figure 6. Inhibition of CYP4Z1-mediated AA metabolism in T47D whole cells by **7**. LC-MS/MS chromatograms showing the AA metabolite profile from CYP4Z1-T47D cells treated with DMSO vehicle (bottom trace) or inhibitor **7** (middle trace), and Vector-T47D cells treated with vehicle (top trace). Cells were treated with 3 μM of **7**, or vehicle, and underwent a 24-hour pre-incubation prior to addition of 50 μM AA, which was followed by a 2-hour incubation for substrate metabolism. This resulted in 14,15-EET, 19-HETE, and 14,15-DiHET metabolite formation being inhibited 83, 86, and 80%, respectively, as compared to vehicle treated CYP4Z1-T47D cells. Vector-T47D cells dosed with vehicle and 50 μM AA showed a minimal amount of background AA metabolism.

Table 4. Inhibition of AA Metabolite Formation in CYP4Z1-T47D Cells by 7

[7] (μM)	14,15-EET		19-HETE		14,15-DiHET	
	minus[a]	*plus*[b]	*minus*	*plus*	*minus*	*plus*
1	47%	70%	41%	73%	25%	59%
3	56%	83%	55%	86%	42%	80%

[a] *Minus* pre-incubation with **7**
[b] *Plus* 24-hour pre-incubation with **7**

Table of Contents Graphic